DETERMINING THE ENERGY PROFILE AND POLYMORPHS OF 6,13-TIPS PENTACENE *IN VACUO* AND IN SOLVENT

A Thesis

Presented to the Faculty of the Graduate School

of Cornell University

In Partial Fulfillment of the Requirements for the Degree of

Master of Science

by

Kristina Marie Lenn

January 2015

ABSTRACT

Organic semiconducting materials are gaining popularity as solar cell materials, in large part because of their ability to be processed onto flexible substrates and to be manufactured more cheaply. However, organic materials are not nearly as efficient as silicon in regards to charge transport. To circumvent this, a process called solution shearing on 6,13-bis(triisopropylsilylethynyl) pentacene (6,13-TIPS pentacene) significantly reduces the pi-orbital overlap, thereby enhancing the charge transport by an 80% increase.

To fully appreciate what is happening at an atomic level and how shearing the unit cell to conform to a configuration that is both energetically favorable and conducive to charge transport, an atomically explicit model of molecules of 6,13-TIPS pentacene were analyzed via *ab initio* and Molecular Dynamics techniques. *In vacuo*, the parameters of the unit cell [a,b,γ] were varied and subjected to minimization calculations, which yielded an energy profile. From this profile, we were able to identify the five lowest energy configurations which were well aligned with the five polymorphs determined experimentally.

Closer examination of the molecular configurations suggested that the fluctuations in the energy profile were due to the bending and twisting of the acene backbone, the wagging of the silylethynyl groups, and the rotating of the methyl groups. Compared to an equilibrium structure, there is a 4.5° deviation in the acene backbone and a

nearly 10° difference in the silylethynyl angle across this energy landscape. However, when comparing the changes in these different angles against the energy profile, the minima for both are closely aligned.

The crystal was also studied in ten different solvents represented by a Lennard-Jones atom, which varied only in size. The new structure was submitted to energy minimization calculations. From this data, it was determined that as the solvent size increases, the stability of the unit cell decreases.

Based on the data gathered, the energy profile of 6,13-TIPS pentacene is significantly affected by the rotating, wagging, and bending of the various side groups and the acene backbone. Whether these deviations occur in sync or are a result of a "domino effect" is not yet clear. The size of the solvent also impacts the energy profile; as the solvent radius increases, the molecules in the unit cell can be seen to almost push at the solvent in an effort to expel it from the unit cell.

BIOGRAPHICAL SKETCH

Kristina Lenn is originally from Detroit, Michigan, where she completed her Bachelor of Science in chemical engineering at Wayne State University.

This work is dedicated to my father, James Lenn, who not only encouraged me to pursue engineering but also has encouraged me to pursue my dreams, grow in my faith, and live with no regrets. I am so happy to be following in his legacy and am proud to say that I am my father's daughter.

ACKNOWLEDGMENTS

First, I would like to thank Dr. Paulette Clancy, my thesis advisor, for her patience and guidance. Also, thank you to Dr. Fernando Escobedo for serving on my committee and for his input. I would also like to acknowledge Dr. Zhenan Bao from Stanford University and her students who provided all of the experimental data for this project.

A special thanks to the Cornell Graduate School, the Semicondcutor Research Corporation, and the Intel Corporation for funding my research. I would especially like to thank my classmates and all the members of the Clancy Research Group for making the last three years more enjoyable. Also, I want to thank the faculty and staff in the College of Engineering at Wayne State University, especially Dr. Jeffrey Potoff for inspiring and encouraging me to attend graduate school and Mrs. Andrea Eisenberg for her guidance, support, and friendship. And finally, I would like to thank my amazing family for all of their support and encouragement. To my big brothers, my favorite guys: Jim, Dan, and Dave, I love you so much and am grateful that you are not only brothers to me but also some of my best friends. To my beautiful sisters-in-law: Heidi, Renee, and Lauren, thank you for marrying into this crazy family and making it more complete. I love you and cannot wait for the Four Fabulous Lenn Ladies to be together again. To my nieces, the light of my life: Sydney, Sophia, Serena, and Samantha, being a part of your growing up is a privilege; I cannot even begin to tell you how much joy you have brought to our family. To my best friends who have become like sisters to me: Sura Peter, Lina Aboulmouna, and Christina Martoni, you are answers to prayer; “the heartfelt counsel of a friend is as sweet as perfume and incense.” To my wonderful parents: words of gratitude seem trivial compared to how much you have invested in my life. I love you and hope I leave as big an impact on others' lives as you have on mine. Mom: “Her children rise up and

call her blessed. Honor her for all that her hands have done." Dad: "The mouth of the righteous man utters wisdom, and his tongue speaks what is just."

TABLE OF CONTENTS

CHAPTER 1

INTRODUCTION

Semiconducting materials are of great importance to today's society because of their many applications ranging from solar cells [1-24] to light-emitting diodes [25-49] to field-effect transistors [50-80]. Semiconductors differ from metals and insulators because of their conductivities [81]; these conductivities are mediated by the presence and size of the material's band gap, which is the energy required to excite an electron from the valence band to the conduction band [82]. If there is no band gap (*i.e.*, the valence and lowest unoccupied bands overlap), the material is a metal (or a conductor) [82]. Semiconductors are classified as having a band gap between the valence and conducting bands ranging from 0.5 to 3 eV [82]. Insulators have band gaps greater than 3 eV and cannot conduct charge at room temperature [82]. The focus of this work will be on the application of semiconducting materials, especially organic semiconductors, for solar cells.

Solar energy is an attractive means of providing power; the promise of having an energy source that cannot be depleted and of being more environmentally friendly than fossil fuels makes them very attractive to the global demand market [83-90]. Whether the economics of solar cell implementation are viable is a subject of great interest but beyond the scope of this fundamentals-based study. The fundamental principle behind solar cells is that when a semiconducting material absorbs a photon of light, the photon excites electrons to a higher energy state and leaves behind “holes” (see **Figure 1.1**). However, instead of immediately relaxing back to the ground state,

the electrons remain in an excited state and induce an electromotive force in the circuit [82]. The more closely the electron and the hole it leaves behind interact, the less efficient the charge transport will be [82]. The Coulombic effects between holes and electrons of the same crystal wave vector yield excitons [82]. Usually at room temperature, the binding energy is low [82]; however, as will be discussed later in this chapter, excitonic binding energy in organic materials is very high [91]. In this case, after the material absorbs a photon and generates excitons, the charges can be split at the junction (an interface between two layers of the same material [homojunction] or between two layers of different materials [heterojunction]) [82]. However, if the excitons have a high binding energy, the charges may recombine prior to arriving at the junction [82]. Efforts made to improving charge transport in organic materials are discussed later.

A variety of different materials are being used, or explored for use, as solar cells. While silicon is, by far, the market leader [92], there has been considerable interest in inorganic photovoltaic materials such as cadmium telluride, copper indium gallium diselenide (CIGS), and various forms of silicon, all of which have band gaps close to the ideal band gap of 1.5 eV [92]. Dye-sensitized materials such as titanium oxide [93-99] and polymers used in conjunction with inorganic materials [100-106] The most commonly deployed and most efficient solar cell material is silicon [107-110] due to its purity [111], abundance, and energy band gap (1.12 eV) [112-113]. The highest limit efficiency achieved by laboratory silicon solar cells is 25% [114]; the Shockley-Queisser limit for silicon solar cells, which is a theoretical estimate of the maximum efficiency to convert sunlight to electricity [115] is around 30% [114].

Recent years have seen the rise of organic semiconducting materials used as the active layers in solar cells. Their light weight [116-121], suitability for cheaper manufacturing via roll-to-roll processing [122-128], ability to be processed on flexible substrates [116] and to be tailored to meet the demands for specific properties [129] make organic semiconductor materials a strong future contender as a solar cell material. However, the biggest drawback for organic solar cells is their low efficiency. Green *et al*. reported that an organic thin film system achieved an efficiency of around 10% [130], which is unusually high. Typically, organic semiconductor materials only obtain around 5 – 6% efficiency [22,129,131-134].

This low solar efficiency is due to the nature of the bonding, the presence of relatively strongly bound excitons, and the mechanism for charge transport via a "hopping" mechanism [91]. Both organic and inorganic materials can exhibit covalent bonding; however, the presence of van der Waals interactions in organic materials leads to a localized wave function and narrow bandwidth. Also, a significant amount of energy (around 0.4 eV) is required to break the exciton binding in organic materials, whereas the potential energy between electrons and holes in inorganic materials does not even equal the thermal energy. Additionally, charge transport in organic materials occurs is largely visualized as occurring via a hopping mechanism, which reduces the charge mobility [91].

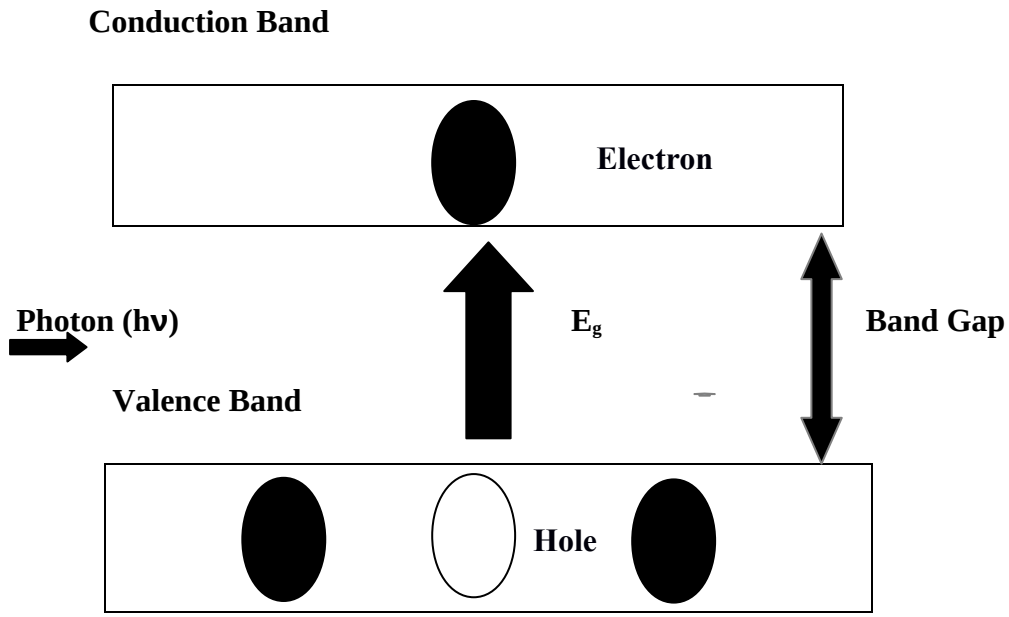

Figure 1.1. Schematic of charge transport from the valence band to the conduction band in a semiconductor upon absorption of a photon.

The focus of most organic semiconducting research efforts has been aimed at increasing the efficiency of the material. Organic semiconducting materials used for solar cells include dye-sensitized, polymeric, and so-called “small-molecule” organic semiconductors. In dye-sensitized organic semiconductors, the charge separation occurs at the junction between an oxide layer and the sensitizer; when the dye absorbs a photon, an electron is excited, and the sensitizer inhibits the recombination of the electron with the dye [135]. Some commonly used sensitizers include RuL' (L' = 2,2',2"-terpyridyl-4,4',4"-tricarboxylic acid) and RuL_3 (L = 2,2'-bipyridyl-4,4'-dicarboxylic acid) joined with a titanium oxide layer [136].

Many polymeric organic semiconductors have band gaps around 2 eV; however, combining a conjugated polymer with fullerene has been shown to overcome the exciton binding energy almost seven orders of magnitude faster than photoluminescence [137]. Some polymer semiconductors include poly[2-methoxy-5-(3',7'-dimethyloctyloxy)-1,4-phenylene vinylene) (MDMO-PPV), poly(3-alkylthiophene) (P3AT), and fullerene derivatives such as 1-(3-methoxycarbonyl)propyl-1-phenyl-[6,6]-methanofullerence (PCBM) [137]. Small molecules like fullerene and phthalocyanine, for example, have an advantage over polymer semiconductors because of their higher purity and structure. Fused acenes are a type of small-molecule organic semiconductor with reasonable electron mobilities. Two of the more important members of this acene family are tetracene and one of the most popular organic solar cell materials, pentacene [138].

Pentacene's hole mobility of over 1 $cm^2 V^{-1} s^{-1}$ [138], comparable to that of amorphous silicon [139]; this makes it an ideal candidate for a solar cell material,

especially considering the notoriety of organic semiconductor materials for exhibiting poor charge mobility. It is a p-type semiconductor [138] and is typically used in conjunction with fullerene, which Sakai *et al*. reported as having a more efficient exciton dissociation leading to enhanced charge transport via alternating-evaporation-deposited active layers [140].

However, pentacene is not very soluble in common solvents which makes solution processing challenging [141]. In addition, herringbone packing structure does not offer a particularly optimized path for charge transport [142], providing the impetus to functionalize pentacene to increase π-stacking and thus enhance charge transport [142-143]. The π-π interactions control crystal packing in these molecules [144] and the desired output is to induce a geometry that will increase orbital overlap, which will lead to better charge transport [143, 145].

One method of functionalizing pentacene that has been studied via perfluorination [146]. However, while perfluoropentacene does exhibit a shorter distance between the pentacene backbones, it also adopts a herringbone structure and has a hole mobility of 0.22 $cm^2 V^{-1} s^{-1}$, which is significantly lower than the mobility of unsubstituted pentacene. Substituting the 6 and 13 positions of pentacene (see **Figure 1.2** [122]) with phenyl groups yielded a molecule with a hole mobility of only 0.1 $cm^2 V^{-1} s^{-1}$ and a larger distance between the pentacene backbones, which impedes the charge transfer. Another functionalization method involved adding alkynes to the pentacene backbone and controlling the stacking structure via the size of the substituent [146].

Substitution of alkyne groups that measured either less than half or greater than

half the length of a pentacene molecule (~1.5 nm) were found to yield slipped-stacked structures [146]. Alkynes that are even longer than those produce the herringbone motif [146] (see **Figure 1.3** [142]), just like unsubstituted pentacene. However, substitution of an alkyne group that measured around half the length of a pentacene molecule gave rise to a "bricklayer" structure [146] (see **Figure 1.4a**). The triisopropyl silylethynyl group yields this favorable structure, and even though its hole mobility is less than that of pentacene (0.4 $cm^2 V^{-1} s^{-1}$) [146], it has a resistivity lower than pentacene [142] and its bricklayer structure induces higher π-orbital overlap (see **Figure 1.4b**) [144]. This structure is known as "TIPS pentacene" for its triisopropyl silylethynyl functionalization, and much of the work accomplished to determine the properties of TIPS pentacene has been performed by the synthesis and characterization studies of John Anthony and co-workers [122,142-147].

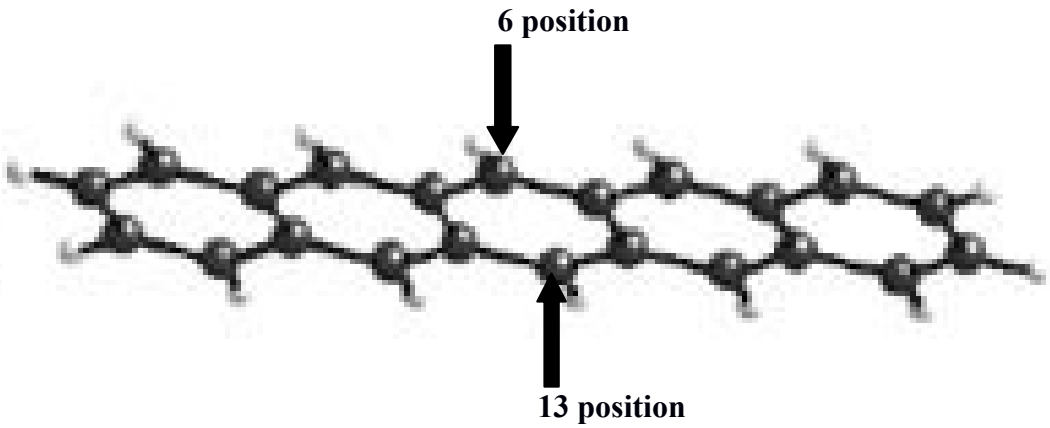

Figure 1.2. Location of the 6 and 13 positions on pentacene, which are the locations of substituents [122].

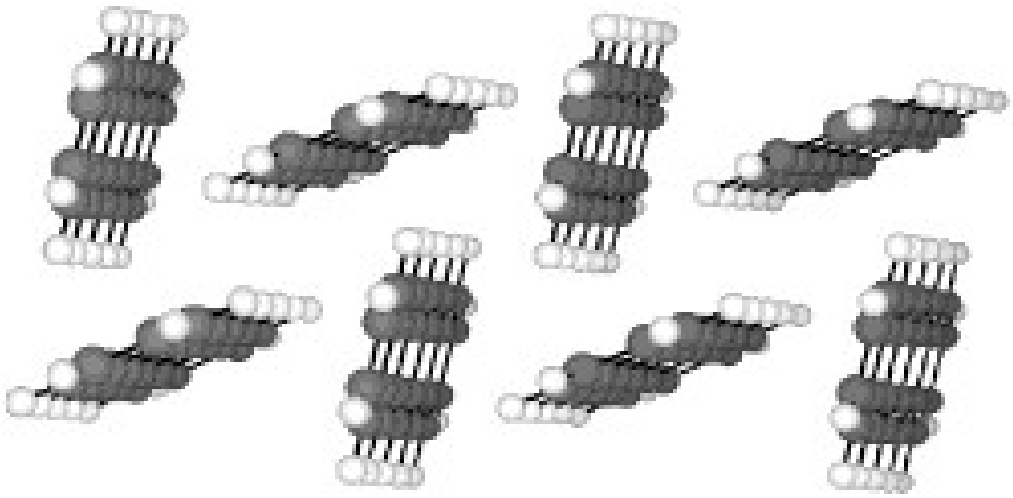

Figure 1.3. Herringbone structure of unsubstituted pentacene [142].

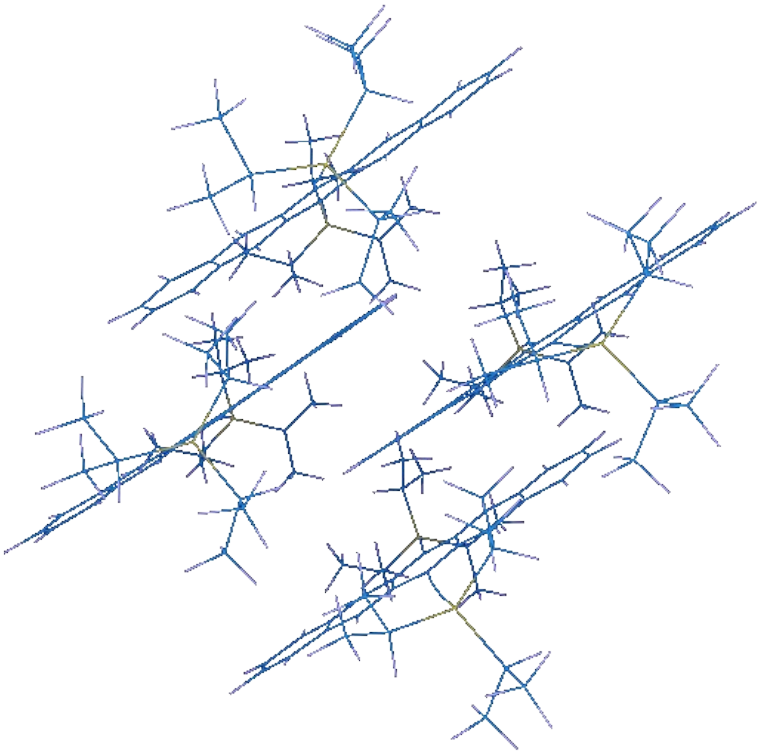

Figure 1.4a. Bricklayer structure of 6,13-TIPS pentacene.

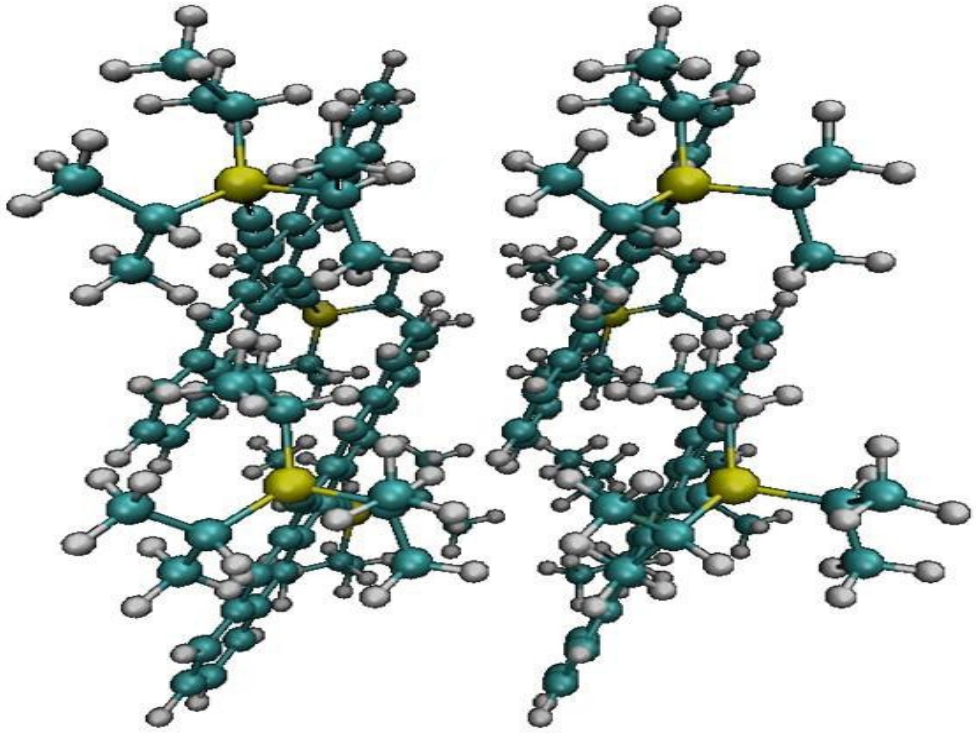

Figure 1.4b. 6,13-TIPS pentacene crystal structure has a bricklayer packing structure that enhances π-orbital overlap, and thereby enhance charge transport.

The electronic properties of TIPS pentacene are known to be impacted by the choice of solution processing method and the accompanying solvent. Park *et al*. discussed some of these methods and stated that the ideal processing method would promote good molecular ordering, which positively impacts the charge transport. Drop casting from a toluene solvent yields the best molecular ordering and an average mobility of 0.65 $cm^2 V^{-1} s^{-1}$ (the highest being 1.8 $cm^2 V^{-1} s^{-1}$); however, films that were drop cast from tetrahydrofuran only achieved a mobility of 0.1 $cm^2 V^{-1} s^{-1}$. Dip-coated films from chlorobenzene yielded mobilities as high as 0.6 $cm^2 V^{-1} s^{-1}$, while spin-cast films from chlorobenzene only reached a mobility around 0.2 $cm^2 V^{-1} s^{-1}$ [147].

However, there exists another method that further increases the charge transport properties of 6,13-TIPS pentacene. Giri *et al*. hypothesized that in order to continue to improve these properties, a similar approach should be taken to that is used in inorganic semiconductors, namely to induce strain into the crystal [148]. To accomplish this, they created a so-called "solution-shearing" method, which uses two silicon plates, one stationary and the other inducing shear in the system. As the top plate (or "doctor blade") moves across the semiconductor, the liquid front evaporates, serving as a "catalyst" for crystal nucleation. One of the most significant impacts of using this method is that the concentration remains constant regardless of the temperature or the deposition time, yielding more uniform films and improved morphologies [148-149].

Dr. Zhenan Bao's group at Stanford found that solution-shearing 6,13-TIPS pentacene caused the π-π stacking distance to decrease significantly, from 3.33 Å to

3.08 Å. The hole mobility also increased from 0.8 $cm^2 V^{-1} s^{-1}$ at a shearing speed of 0.4 mm/s to 4.6 $cm^2 V^{-1} s^{-1}$ at a shearing speed of 2.8 mm/s. Interestingly, and without mechanistic explanation by Giri *et al*., there was a simple means to return the system to a thermodynamically stable state. Toluene was the solvent used in the solution shearing. Once the 6,13-TIPS pentacene had been sheared and the solvent evaporated, toluene vapor was re-introduced into the system, which caused the structure to return to an equilibrium state [148].

The goal of this work is to try to expand upon and understand what occurs during solution shearing at an atomic level. This understanding will allow us to appreciate what mediates the processing-induced transition from one polymorph to another, as manifested in the unit cell parameters of the most stable polymorph for a given shear. Chapter 3 describes the molecular models and simulation methods used in this work. The remaining chapters will discuss how the effects of solvent size affects the energy profile of the 6,13-TIPS pentacene crystal.

REFERENCES

1. Katz, H. E., Z. Bao, S. L. Gilat. "Synthetic Chemistry for Ultrapure, Processable, and High-Mobility Organic Transistor Semiconductors." *Accounts of Chemical Research*, 2001, **34**: 359 – 369.

2. Burn, P. L., A. B. Holmes, A. Kraft, D. D. C. Bradley, A. R. Brown, R. H. Friend, R. W. Gymer. "Chemical tuning of electroluminescent copolymers to improve emission efficiencies and allow patterning." *Letters to Nature*, 1992, **356**: 47 – 49.

3. Vurgaftman, I., J. R. Meyer, L. R. Ram-Mohan. "Band parameters for III-V compound semiconductors and their alloys." *Journal of Applied Physics*, 2001, **89**: 5815 – 5875.

4. Kamat, P. V. "Quantum Dot Solar Cells. Semiconductor Nanocrystals as Light Harvesters." *Journal of Physical Chemistry*, 2008, **112**: 18737 – 18753.

5. Huynh, W. U., J. J. Dittmer, A. P. Alivisatos. "Hybrid Nanorod-Polymer Solar Cells." *Science*, 2002, **29**: 2425 – 2427.

6. Brabec, C. J., N. Serdar Sariciftci, J. C. Hummelen. "Plastic Solar Cells." *Advanced Functional Materials*, 2001, **11**: 15 – 26.

7. Gur, I., N. A. Fromer, M. L. Geier, A. P. Alivisatos. "Air-Stable All-Inorganic Nanocrystal Solar Cells Processed from Solutions." *Science*, 2005, **310**: 462 – 465.

8. Kayes, B. M., H. A. Atwater. "Comparison of the device physics principles of planar and radial *p-n* junction nanorod solar cells." *Journal of Applied Physics*, 2005, **97**: 114302-1 – 114302-11.

9. Gur, I., N. A. Fromer, C-P. Chen, A. G. Kanaras, A. P. Alivisatos. "Hybrid Solar

Cells with Prescribed Nanoscale Morphologies Based on Hyperbranched Semiconductor Nanocrystals." *Nano Letter*, 2007, **7**: 409 – 414.

10. Milliron, D. J., I. Gur, A. P. Alivisatos. "Hybrid Organic-Nanocrystal Solar Cells." *Materials Research Society Bulletin*, 2005, **30**: 41 – 44.

11. Bisquert, J., A. Zaban, M. Greenshtein, I. Mora-Sero. "Determination of Rate Constants for Charge Transfer and the Distribution of Semiconductor and Electrolyte Electronic Energy Levels in Dye-Sensitized Solar Cells by Open-Circuit Photovoltage Decay Method." *Journal of the American Chemical Society*, 2004, **126**: 13550 – 13559.

12. Zaban, A., M. Greenshtein, J. Bisquert. "Determination of the Electron Lifetime in Nanocrystalline Dye Solar Cells by Open-Circuit Voltage Decay Measurements." *ChemPhysChem*, 2003, **4**: 859 – 864.

13. J. Bisquert. "Chemical capacitance of nanostructured semiconductors: its origin and significance for nanocomposite solar cells." *Physical Chemistry Chemical Physics*, 2003, **5**: 5360 – 5364.

14. Gregg, B. A. "Excitonic Solar Cells." *Journal of Physical Chemistry B*, 2003, **107**: 4688 – 4698.

15. Bisquert, J., V. S. Vikhrenko. "Interpretation of the Time Constants Measured by Kinetic Techniques in Nanostructured Semiconductor Electrodes and Dye-Sensitized Solar Cells." *Journal of Physical Chemistry B*, 2004, **108**: 2313 – 2322.

16. Baxter, J., E. S. Aydil. "Nanowire-based dye-sensitized solar cells." *Applied Physics Letters*, 2005, **86**: 053114-1 – 053114-3.

17. Catchpole, K. R., A. Polman. "Plasmonic solar cells." *Optics Express*, 2008, **16**:

21793 – 21800.

18. Gratzel, M. “Perspectives for Dye-sensitized Nanocrystalline Solar Cells.” *Progress in Photovoltaics Research and Applications*, 2000, **8**: 171 – 185.

19. Nozik, A. J., M. C. Beard, J. M. Luther, M. Law, R. J. Ellingson, J. C. Johnson. “Semiconductor Quantum Dots and Quantum Dot Arrays and Applications of Multiple Exciton Generation to Third-Generation Photovoltaic Solar Cells.” *Chemical Reviews*, 2010, **110**: 6873 – 6890.

20. Rand, B. P., J. Genoe, P. Heremans, J. Poortmans. “Solar Cells Utilizing Small Molecular Weight Organic Semiconductors.” *Progress in Photovoltaics Research and Applications*, 2007, **15**: 659 – 676.

21. Hodes, G. “Comparison of Dye- and Semiconductor-Sensitized Porous Nanocrystalline Liquid Junction Solar Cells.” *Journal of Physical Chemistry C*, 2008, **112**: 17778 – 17787.

22. Kim, J. Y., K. Lee, N. E. Coates, D. Moses, T-Q. Nguyen, M. Dante, A. J. Heeger. “Efficient Tandem Polymer Solar Cells Fabricated by All-Solution Processing.” *Science*, 2007, **317**: 222 – 225.

23. Jiang, C. Y., X. W. Sun, G. Q. Lo, D. L. Kwong. “Improved dye-sensitized solar cells with a ZnO-nanoflower photoanode.” *Applied Physics Letters*, 2007, **90**: 263501-1 – 263501-3.

24. Kamat, P. V., K. Tvrdy, D. R. Baker, J. G. Radich. “Beyond Photovoltaics: Semiconductor Nanoarchitectures for Liquid-Junction Solar Cells.” *Chemical Reviews*, 2010, **110**: 6664 – 6688.

25. Burroughes, J. H., D. D. C. Bradley, A. R. Brown, R. N. Marks, K. Mackay, R. H.

Friend, P. L. Burns, A. B. Holmes. “Light-emitting diodes based on conjugated polymers.” *Nature*, 1990, **347**: 539 – 541.

26. Waltereit, P., O. Brandt, A. Trampert, H. T. Grahn, J. Menniger, M. Ramsteiner, M. Reiche, K. H. Ploog. “Nitride semiconductors free of electrostatic fields for efficient white light-emitting diodes.” *Nature*, 2000, **406**: 865 – 868.

27. Ponce, F. A., D. P. Bour. “Nitride-based semiconductors for blue and green light-emitting devices.” *Nature*, 1997, **386**: 351 – 359.

28. Colvin, V. L., M. C. Schlamp, A. P. Alivisatos. “Light-emitting diodes made from cadmium selenide nanocrystals and a semiconducting polymer.” *Nature*, 1994, **370**: 354 – 357.

29. Kish, F. A., F. M. Steranka, D. C. DeFevere, D. A. Vanderwater, K. G. Park, C. P. Kuo, T. D. Osentowski, M. J. Peanasky, J. G. Yu, R. M. Fletcher, D. A. Steigerwald, M. G. Craford, V. M. Robbins. “Very high-efficiency semiconductor wafer-bonded transparent-substrate $(Al_xGa_{1-x})_{0.5}In_{0.5}P$/GaP light-emitting diodes.” *Applied Physics Letters*, 1994, **64**: 2839 – 2841.

30. Pfeiffer, M., K. Leo, X. Zhou, J. S. Huang, M. Hofmann, A. Werner, J. Blochwitz-Nimoth. “Doped organic semiconductors: Physics and application in light emitting diodes.” *Organic Electronics*, 2003, **4**: 89 – 103.

31. Green, M. A., J. Zhao, A. Wang, P. J. Reece, M. Gal. “Efficient silicon light-emitting diodes.” *Nature*, 2001, **412**: 805 – 808.

32. Krames, M. R., O. B. Shchekin, R. Mueller-Mac, G. O. Mueller, L. Zhou, G. Harbers, M. G. Craford. “Status and Future of High-Power Light-Emitting Diodes for Solid-State Lighting.” *Journal of Display Technology*, 2007, **3**: 160 – 175.

33. Schubert, E. F., N. E. J. Hunt, M. Micovic, R. J. Malik, D. L. Sivco, A. Y. Cho, G. J. Zydzik. “Highly Efficient Light-Emitting Diodes with Microcavities.” *Science*, 1994, **265**: 943 – 945.

34. Rogach, A. L., N. Gaponik, J. M. Lupton, C. Bertoni, D. E. Gallardo, S. Dunn, N. L. Pira, M. Paderi, P. Repetto, S. G. Romanov, C. O'Dwyer, C. M. Sotomayor Torres, A. Eychmuller. “Light-Emitting Diodes with Semiconductor Nanocrystals.” *Angewandte Chemie International Edition*, 2008, **47**: 6538 – 6549.

35. Schlamp, M. C., X. Peng, A. P. Alivisatos. “Improved efficiencies in light emitting diodes made with CdSe(CdS) core/shell type nanocrystals and a semiconducting polymer.” *Jouranl of Applied Physics*, 1997, **82**: 5837 – 5842.

36. Heidenhain, S. B., Y. Sakamoto, T. Suzuki, A. Miura, H. Fujikawa, T. Mori, S. Tokito, Y. Taga. “Perfluorinated Oligo(*p*-Phenylene)s: Efficient n-Type Semiconductors for Organic Light-Emitting Diodes.” *Journal of American Chemical Society*, 2000, **122**: 10240 – 10241.

37. Kim, J-S., R. H. Friend, I. Grizzi, J. H. Burroughes. “Spin-cast thin semiconducting polymer interlayer for improving device efficiency of polymer light-emitting diodes.” *Applied Physics Letters*, 2005, **87**: 023506-1 – 023506-3.

38. Parker, I. D. “Carrier tunneling and device characteristics in polymer light-emitting diodes.” *Journal of Applied Physics*, 1994, **75**: 1656 – 1666.

39. Erchak, A. A., D. J. Ripin, S. Fan, P. Rakich, J. D. Joannopoulos, E. P. Ippen, G. S. Petrich, L. A. Kolodziejski. “Enhanced coupling to vertical radiation using a two-dimensional photonic crystal in a semiconductor light-emitting diode.” *Applied Physics Letters*, 2001, **78**: 563 – 565.

40. Nakamura, S., M. Senoh, T. Mukai. “High-power InGaN/GaN double-heterostructure violet light emitting diodes.” *Applied Physics Letters*, 1993, **62**: 2390 – 2392.

41. Sun, X., J. Liu, L. C. Kimerling, J. Michel. “Room-temperature direct bandgap electroluminescence from Ge-on-Si light-emitting diodes.” *Optics Letters*, 2009, **34**: 1198 – 1200.

42. Chhajed, S., Y. Xi, Y-L. Li, T. Gessmann, E. F. Schubert. “Influence of junction temperature on chromaticity and color-rendering properties of trichromatic white-ligth sources based on light-emitting diodes.” *Journal of Applied Physics*, 2005, **97**: 054506-1 – 054506-8.

43. Kim, H-M., Y-H. Cho, H. Lee, S. I. Kim, S. R. Ryu, D. Y. Kim, T. W. Kang, K. S. Chung. “High-Brightness Light Emitting Diodes Using Dislocation-Free Indium Gallium Nitride/Gallium Nitride Multiquantum-Well Nanorod Arrays.” *Nano Letters*, 2004, **4**: 1059 – 1062.

44. Tessler, N., V. Medvedev, M. Kazes, S. Kan, U. Banin. “Efficient Near-Infrared Polymer Nanocrystal Light-Emitting Diodes.” *Science*, 2002, **295**: 1506 – 1508.

45. Delbeke, D., R. Bockstaele, P, Bienstman, R. Baets, H. Benisty. “High-Efficiency Semiconductor Resonant-Cavity Light-Emitting Diodes: A Review.” *IEEE Journal on Selected Topics in Quantum Electronics*, 2002, **8**: 189 – 206.

46. Kulkarni, A. P., C. J. Tonzola, A. Babel, S. A. Jenekhe. “Electron Transport Materials for Organic Light-Emitting Diodes.” *Chemical Materials*, 2004, **16**: 4556 – 4573.

47. Marteani, A. C., A. S. Dhoot, J-S. Kim, C. Silva, N. C. Greenham, C. Murphy, E.

Moons, S. Cina, J. H. Burroughes, R. H. Friend. “Barrier-Free Electron-Hole Capture in Polymer Blend Heterojunction Light-Emitting Diodes.” *Advanced Materials*, 2003, **15**: 1708 – 1712.

48. Horng, R. H., C. C. Yang, J. Y. Wu, S. H. Huang, C. E. Lee, D. S. Wuu. “GaN-based light-emitting diodes with indium tin oxide texturing window layers using natural lithography.” *Applied Physics Letters*, 2005, **86**: 221101-1 – 221101-3.

49. Gotz, W., R. S. Kern, C. H. Chen, H. Liu, D. A. Steigerwald, R. M. Fletcher. “Hall-effect characterization of III-V nitride semiconductors for high efficiency light emitting diodes.” *Materials Science and Engineering B*, 1999, **59**: 211 – 217.

50. Hung, K. K., P. K., Ko, H. Chenming, Y. C., Cheng. “A unified model for the flicker noise in metal-oxide-semiconductor field-effect transistors.” *Electron Devices*, 1990, **37**: 654 – 665.

51. Lee, M. L., E. A. Fitzgerald, M. T. Bulsara, M. T. Currie, A. Lochtefeld. “Strained Si, SiGe, and Ge channels for high-mobility metal-oxide-semiconductor field-effect transistors.” *Journal of Applied Physics*, 2005, **97**: 011101-1 – 011101-27.

52. Welser, J., J. L. Hoyt, J. F. Gibbons. “Electron mobility enhancement in strained-Si n-type metal-oxide-semiconductor field-effect transistors.” *Electron Device Letters*, 1994, **15**: 100 – 102.

53. Ren, F., M. Hong, S. N. G. Chu, M. A. Marcus, M. J. Schurman, A. Baca, S. J. Pearton, C. R. Abernathy. “Effect of temperature on $Ga_2O_3(Gd_2O_3)$/GaN metal-oxide-semiconductor field-effect transistors.” *Applied Physics Letters*, 1998, **73**: 3893 – 3895.

54. Takagi, S., J. L. Hoyt, J. J. Welser, J. F. Gibbons. “Comparative study of

phononlimited mobility of two-dimensional electrons in strained and unstrained Si metal-oxide-semiconductor field-effect transistors." *Journal of Applied Physics*, 1996, **80**: 1567 – 1577.

55. Lee, M. L., C. W. Leitz, Z. Cheng, A. J. Pitera. "Strained Ge channel p-type metal-oxide-semiconductor field-effect transistors grown on $Si_{1-x}Ge_x$/Si virtual substrates." *Applied Physics Letters*, 2001, **79**: 3344 – 3346.

56. Brown, A. R., A. Pomp, D. M. de Leeuw, D. B. M. Klaassen, E. E. Havinga, P. Herwig, K. Mullen. "Precursor route pentacene metal-insulator-semiconductor field-effect transistors." *Journal of Applied Physics*, 1996, **79**: 2136 – 2138.

57. Brown, A. R., C. P. Jarrett, D. M. de Leeuw, M. Matters. "Field-effect transistors made from solution-processed organic semiconductors." *Synthetic Metals*, 1997, **88**: 37 – 55.

58. Wang, C., J. P. Snyder, J. R. Tucker. "Sub-40 nm PtSi Schottky source/drain metal-oxide-semiconductor field-effect transistors." *Applied Physics Letters*, 1999, **74**: 1174 – 1176.

59. Wind, S. J., J. Appenzeller, R. Martel, V. Derycke, P. Avouris. "Vertical scaling of carbon nanotube field-effect transistors using top gate electrodes." *Applied Physics Letters*, 2002, **80**: 3817 – 3819.

60. Uren, M. J., D. J. Day, M. J. Kirton. "1/f and random telegraph noise in silicon metal-oxide-semiconductor field-effect transistors." *Applied Physics Letters*, 1995, **47**: 1195 – 1197.

61. Bao, Z., A. J. Lovinger, A. Dodabalapur. "Organic field-effect transistors with high mobility based on copper phthalocyanine." *Applied Physics Letters*, 1996, **69**:

3066 – 3068.

62. Lim, S-G., S. Kriventsov, T. N. Jackson, J. H. Haeni, D. G. Schlom, A. M. Balbashov, R. Uecker, P. Reiche, J. L. Freeouf, G. Lucovsky. “Dielectric functions and optical bandgaps of high-K dielectrics for metal-oxide-semiconductor field-effect transistors by far ultraviolet spectroscopic ellipsometry.” *Journal of Applied Physics*, 2002, **91**: 4500 – 4505.

63. Natori, K. “Ballistic metal-oxide-semiconductor field effect transistor.” *Journal of Applied Physics*, 1994, **76**: 4879 – 4891.

64. Sun, Y., S. E. Thompson, T. Nishida. “Physics of strain effects in semiconductors and metal-oxide-semiconductor field-effect transistors.” *Journal of Applied Physics*, 2007, **98**: 104503-1 – 104503-22.

65. Ershov, M., S. Saxena, H. Karbasi, S. Winters, S. Minehane, J. Babcock, R. Lindley, P. Clifton, M. Redford, A. Shibkov. “Dynamic recovery of negative bias temperature instability in *p*-type metal-oxide-semiconductor field-effect transistors.” *Applied Physics Letters*, 2003, **83**: 1647 – 1649.

66. Khan, M. A., J. N. Kuznia, A. R. Bhattarai, D. T. Olson. “Metal semiconductor field effect transistor based on single crystal GaN.” *Applied Physics Letters*, 1993, **62**: 1786 – 1787.

67. Ye, P. D., G. D. Wilk, B. Yang, J. Kwo, S. N. G. Chu, S. Nakahara, H.-J. L. Gossmann, J. P. Mannaerts, M. Hong, K. K. Ng, J. Bude. “GaAs metal-oxide-semiconductor field-effect transistor with nanometer-thin dielectric grown by atomic layer deposition.” *Applied Physics Letters*, 2003, **83**: 180 – 182.

68. Allard, S., M. Forster, B. Souharce, H. Thiem, U. Scherf. “Organic

Semiconductors for Solution-Processable Field-Effect Transistors (OFETs)." *Angerwandte Chemi International Edition*, 2008, **47**: 4070 – 4098.

69. Leitz, C. W., M. T. Currie, M. L. Lee, Z.-Y. Cheng, D. A. Antoniadis, E. A. Fitzgerald. "Hole mobility enhancements in strained $Si/Si_{1-y}Ge_y$ p-type metal-oxide-semiconductor field-effect transistors grown on relaxed $Si_{1-x}Ge_x$ ($x<y$) virtual substrates." *Applied Physics Letters*, 2001, **79**: 4246 – 4248.

70. Leitz, C. W., M. T. Currie, M. L. Lee, Z.-Y. Cheng, D. A. Antoniadis, E. A. Fitzgerald. "Hole mobility enhancements and alloy scattering-limited mobility in tensile strained Si/SiGe surface channel metal-oxide-semiconductor field-effect transistors." *Journal of Applied Physics*, 2002, **92**: 3745 – 3751.

71. Kobayashi, S., T. Nishikawa, T. Takenobu, S. Mori, T. Shimoda, T. Mitani, H. Shimotani, N. Yoshimoto, S. Ogawa, Y. Iwasa. "Control of carrier density by self-assembled monolayers in organic field-effect transistors." *Nature Materials*, 2004, **3**: 317 – 322.

72. Kagan, C. R., D. B. Mitzi, C. D. Dimitrakopoulos. "Organic-Inorganic Hybrid Materials as Semiconducting Channels in Thin-Film Field-Effect Transistors." *Science*, 1999, **286**: 945 – 947.

73. Klein, P. B., J. A. Freitas, Jr., S. C. Binari, A. E. Wickenden. "Observation of deep traps responsible for current collapse in GaN metal-semiconductor field-effect transistors." *Applied Physics Letters*, 1999, **75**: 4016 – 4018.

74. Metze, G. M., H. K. Choi, BY. Tsaur. "Metal-semiconductor field-effect transistors fabricated in GaAs layers grown directly on Si substrates by molecular beam epitaxy." *Applied Physics Letters*, 1984, **45**.

75. Uchida, K., S-I. Takagi. “Carrier scattering induced by thickness fluctuation of silicon-on-insulator film in ultrathin-body metal-oxide-semiconductor field-effect transistors.” *Applied Physics Letters*, 2003, **82**: 2916 – 2918.

76. Sugahara, S., M. Tanaka. “A spin metal-oxide-semiconductor field-effect transistor using half-metallic-ferromagnet contacts for the source and drain.” *Applied Physics Letters*, 2004, **84**: 2307 – 2309.

77. Gardelis, S., C. G. Smith, C. H. W. Barnes, E. H. Linfield, D. A. Ritchie. “Spin-valve effects in a semiconductor field-effect transistor: A spintronic device.” *Physical Review B*, 1999, **60**: 7764 – 7767.

78. Appenzeller, J., Y.-M. Lin, J. Knoch, P. Avouris. “Band-to-Band Tunneling in Carbon Nanotube Field-Effect Transistors.” *Physical Review Letters*, 2004, **93**: 196805-1 – 196805-4.

79. Hu, X., A. Koudymov, G. Simin, J. Yang, M. Asif Khan, A. Tarakji, M. S. Shur, R. Gaska. “Si_3N_4 AlGaN GaN-metal-insulator-semiconductor heterostructure field-effect transistors.” *Applied Physics Letters*, 2001, **79**: 2832 – 2834.

80. Knoch, J., J. Appenzeller. “Impact of the channel thickness on the performance of Schottky barrier metal-oxide-semiconductor field-effect transistors.” *Applied Physics Letters*, 2002, **81**: 3082 – 3084.

81. Talley, H. E., D. G. Daughtery. *Physical Principles of Semiconductor Devices*. Ames: Iowa State University Press, 1976.

82. Nelson, J. *The Physics of Solar Cells*. London: Imperial College Press, 2003.

83. Goetzberger, A., C. Hebling, H.-W. Schock. “Photovoltaic materials, history, status and outlook.” *Materials Science and Engineering*, 2003, **40**: 1 – 46.

84. Garnett, E. C., P. Yang. “Silicon Nanowire Radial p-n Junction Solar Cells.” *Journal of the American Chemical Society*, 2008, **130**: 9224 – 9225.

85. Gratzel, M. “Mesoscopic Solar Cells for Electricity and Hydrogen Production from Sunlight.” *Chemistry Letters*, 2005, **34**: 8 – 13.

86. Gratzel, M. “Recent Advances in Sensitized Mesoscopic Solar Cells.” *Accounts of Chemical Research*, 2009, **42**: 1788 – 1798.

87. Turner, J. A. “A Realizable Renewable Energy Future.” *Science*, 1999, **285**: 687 – 689.

88. Lewis, N. S., D. G. Nocera. “Powering the planet: Chemical challenges in solar energy utilization.” *Proceedings of the National Academy of Sciences*, 2006, **103**: 15729 – 15735.

89. Crabtree, G. W., N. S. Lewis. “Solar energy conversion.” *American Institute of Physics*, 2007, **60**: 37 – 42.

90. Gust, D., T. A. Moore, A. L. Moore. “Solar Fuels via Artificial Photosynthesis.” *Accounts of Chemical Research*, 2009, **42**: 1890 – 1898.

91. Goh, C., M. D. McGehee. “Organic Semiconductors for Low-Cost Solar Cells.” *The Bridge: National Academy of Engineering of the National Academies*, 2005, **35**: 33 – 39.

92. Miles, R. W., G. Zoppi, I. Forbes. “Inorganic photovoltaic cells.” *Materials Today*, 2007, **10**: 20 – 27.

93. O'Regan. B., M. Gratzel. “A low-cost, high-efficiency solar based on dye-sensitized colloidal TiO_2 films.” *Nature*, 1991, **353**: 737 – 740.

94. Bach, U., D. Lupo, P. Comte, J. E. Moser, F. Weissortel, J. Salbeck, H. Spreitzer,

M. Gratzel. "Solid-state dye-sensitized mesoporous TiO_2 solar cells with high photon-to-electron conversion efficiencies." *Nature*, 1998, **395**: 583 – 585.

95. Bisquert, J., V. S. Vikhrenko. "Interpretation of the Time Constants Measured by Kinetic Techniques in Nanostructured Semiconductor Electrodes and Dye-Sensitized Solar Cells." *Journal of Physical Chemistry B*, 2004, **108**: 2313 – 2322.

96. Gratzel, M. "Solar Energy Conversion by Dye-Sensitized Photovoltaic Cells." *Inorganic Chemistry*, 2005, **44**: 6841 – 6851.

97. Mor, G. K., K. Shankar, M. Paulose, O. K. Varghese, C. A. Grimes. "Use of Highly-Ordered TiO_2 Nanotube Arrays in Dye-Sensitized Solar Cells." *Nano Letters*, 2006, **6**: 215 – 218.

98. Hara, K., K. Sayama, Y. Ohga, A. Shinpo, S. Suga, H. Arakawa. "A coumarin-derivative dye sensitized nanocrystalline TiO_2 solar cell having a high solar-energy conversion efficiency up to 5.6%." *Chemical Communications*, 2001: 569 – 570.

99. Huang, S. Y., G. Schlichthorl, A. J. Nozik, M. Gratzel, A. J. Frank. "Charge Recombination in Dye-Sensitized Nanocrystalline TiO_2 Solar Cells." *Journal of Physical Chemistry B*, 1997, **101**: 2576 – 2582.

100. Huynh, W. U., J. J. Dittmer, A. P. Alivisatos. "Hybrid Nanorod-Polymer Solar Cells." *Science*, 2002, **295**: 2425 – 2427.

101. Xu, T., Q. Qiao. "Conjugated polymer-inorganic semiconductor hybrid solar cells." *Energy and Environmental Science*, 2011, **4**: 2700 – 2720.

102. Leventis, H. C., S. P. King, A. Sudlow, M. S. Hill, K. C. Molloy, S. A. Haque. "Nanostructured Hybrid Polymer-Inorganic Solar Cell Active Layers Formed by Controllable in Situ Growth of Semiconducting Sulfide Networks." *Nano Letters*,

2010, **10**: 1253 – 1258.

103. Ren, S., L-Y. Chang, S-K. Lim, J. Zhao, M. Smith, N. Zhao, V. Bulovic, M. Bawendi, S. Gradecak. "Inorganic-Organic Hybrid Solar Cell: Bridging Quantum Dots to Conjugated Polymer Nanowires." *Nano Letters*, 2011, **11**: 3998 – 4002.

104. Heo, J. H., S. H. Im, J. H. Noh, T. N. Mandal, C-S. Lim, J. A. Chang, Y. H. Lee, H-J. Kim, A. Sarkar, M. K. Nazeerudding, M. Gratzel, S. I. Seok. "Efficient inorganic-organic hybrid heterojunction solar cells containing perovskite compound and polymeric hole conductors." *Nature Photonics*, 2013, **7**: 486 – 491.

105. Beek, W. J. E., M. M. Wienk, R. A. J. Janssen. "Efficient Hybrid Solar Cells from Zinc Oxide Nanoparticles and a Conjugated Polymer." *Advanced Materials*, 2004, **16**: 1009 – 1013.

106. Huynh, W. U., J. J. Dittmer, W. C. Libby, G. L. Whiting, A. P. Alivisatos. "Controlling the Morphology of Nanocrystal-Polymer Composites for Solar Cells." *Advanced Functional Materials*, 2003, **13**: 73 – 79.

107. Sreejith, P. S., G. Udupa, Y. B. M. Noor, B. K. A. Ngoi. "Recent Advances in Machining of Silicon Wafers for Semiconductor Applications." *The International Journal of Advanced Manufacturing Technology*, 2001, **17**: 157 – 162.

108. Goetzberger, A., J. Luther, G. Willeke. "Solar cells: past, present, future." *Solar Energy Materials and Solar Cells*, 2002, **74**: 1 – 11.

109. Bermel, P., C. Luo, L. Zeng, L. C. Kimerling, J. D. Joannopoulos. "Improving thin-film crystalline silicon solar cell efficiencies with photonic crystals." *Optics Express*, 2007, **15**: 16986 – 17000.

110. Tsakalakos, L., J. Balch, J. Fronheiser, B. A. Korevaar, O. Sulima, J. Rand.

"Silicon nanowire solar cells." *Applied Physics Letters*, 2007, **91**: 233117-1 – 233117-3.

111. Fahrenbruch, A. L., R. H. Bube. *Fundamentals of Solar Cells: Photovoltaic Solar Energy Conversion*. New York, Academic Press, Inc., 1983.

112. Tiedje, T., E. Yablonovitch, G. D. Cody, B. G. Brooks. "Limiting Efficiency of Silicon Solar Cells." *IEEE Transactions on Electron Devices*, 1984, **31**: 711 – 716.

113. Strumpel, C., M. McCann, G. Beaucarne, V. Arkhipov, A. Slaoui, V. Svrcek, C. del Canizo, I. Tobias. "Modifying the solar spectrum to enhance silicon solar cell efficiency – An overview of available materials." *Solar Energy Materials and Solar Cells*, 2007, **91**: 238 – 249.

114. Swanson, R. M. "Approaching the 29% Limit Efficiency of Silicon Solar Cells." *IEEE Photovoltaic Specialists Conference*, 2005, **31**: 889 – 894.

115. Hoertz, P. G., A. Staniszewski, A. Marton, G. T. Higgins, C. D. Incarvito, A. L. Rheingold, G. J. Meyer. "Toward Exceeding the Shockley-Queisser Limit: Photoinduced Interfacial Charge Transfer Processes that Store Energy in Excess of the Equilibrated Excited State." *Journal of the American Chemical Society*, 2006, **128**: 8234 – 8245.

116. Hoppe, H., N. S. Sariciftci. "Organic solar cells: An overview." *Journal of Materials Research*, 2004, **19**: 1924 – 1944.

117. Burrows, P. E., G. Gu, V. Bulovic, Z. Shen, S. R. Forrest, M. E. Thompson. "Achieving Full-Color Organic Light-Emitting Devices for Lightweight, Flat-Panel Displays." *IEEE Transactions on Electron Devices*, 1997, **44**: 1188 – 1203.

118. Someya, T., Y. Kato, S. Iba, Y. Noguchi, T. Sekitani, H. Kawaguchi, T. Sakurai.

"Integration of Organic FETs With Organic Photodiodes for a Large Area, Flexible, and Lightweight Sheet Image Scanners." *IEEE Transactions on Electron Devices*, 2005, **52**: 2502 – 2511.

119. Roncali, J., P. Leriche, A. Cravino. "From One- to Three-Dimensional Organic Semiconductors: In Search of the Organic Silicon?" *Advanced Materials*, 2007, **19**: 2045 – 2060.

120. Forrest, S. R. "The path to ubiquitous and low-cost organic electronic appliances on plastic." *Nature*, 2004, **428**: 911 – 918.

121. Chen, F.-C., C.-W. Chu, J. He, Y. Yang. "Organic thin-film transistors with nanocomposite dielectric gate insulator." *Applied Physics Letters*, 2004, **85**: 3295 – 3297.

122. Anthony, J. E. "The Larger Acenes: Versatile Organic Semiconductors." *Angewandte Chemie International Edition*, 2008, **47**: 452 – 483.

123. Pan, H., Y. Li, Y. Wu, P. Liu, B. S. Ong, S. Zhu, G. Xu. "Low-Temperature, Solution-Processed, High-Mobility Polymer Semiconductors for Thin-Film Transistors." *Journal of the American Chemical Society*, 2006, **129**: 4112 – 4113.

124. Gaudiana, R., C. Brabec. "Fantastic plastic." *Nature Photonics*, 2008, **2**: 287 – 289.

125. Galagan, Y., I. G. de Vries, A. P. Langen, R. Andriessen, W. J. H. Verhees, S. C. Veenstra, J. M. Kroon. "Technology development for roll-to-roll production of organic photovoltaics." *Chemical Engineering and Processing: Process Intensification*, 2011, **50**: 454 – 461.

126. Sondergaard, R. R., M. Hosel, F. C. Krebs. "Roll-to-Roll fabrication of large area

functional organic materials." *Journal of Polymer Science Part B*, 2013, **51**: 16 – 34.

127. Becerril, H. A., M. E. Roberts, Z. Liu, J. Locklin, Z. Bao. "High-Performance Organic Thin-Film Transistors through Solution-Sheared Deposition of Small-Molecule Organic Semiconductors." *Advanced Materials*, 2008, **20**: 2588 – 2594.

128. Logothetidis, S. "Flexible organic electronic devices: Materials, process and applications." *Materials Science and Engineering B*, 2008, **152**: 96 – 104.

129. Potscavage, Jr., W. J., A. Sharma, B. Kippelen. "Critical Interfaces in Organic Solar Cells and Their Influence on the Open-Circuit Voltage." *Accounts of Chemical Research*, 2009, **42**: 1758 – 1767.

130. Xue, J., S. Uchida, B. P. Rand, S. R. Forrest. "Asymmetric tandem organic photovoltaic cells with hybrid planar-mixed molecular heterojunctions." *Applied Physics Letters*, 2004, **85**: 5757 – 5759.

131. Ma, W., C. Yang, X. Gong, K. Lee, A. J. Heeger. "Thermally Stable, Efficient Polymer Solar Cells with Nanoscale Control of the Interpenetrating Network Morphology." *Advanced Functional Materials*, 2005, **15**: 1617 – 1622.

132. Peet, J., J. Y. Kim, N. E. Coates, W. L. Ma, D. Moses, A. J. Heeger, G. C. Bazan. "Efficiency enhancement in low-bandgap polymer solar cells by processing with alkane dithiols." *Nature Materials*, 2007, **6**: 497 – 500.

133. Liang, Y., Y. Wu, D. Feng, S-T. Tsai, H-J. Son, G. Li, L. Yu. "Development of New Semiconducting Polymers for High Performance Solar Cells." *Journal of the American Chemical Society*, 2009, **131**: 56 – 57.

134. Green, M. A., K. Emery, Y. Hishikawa, W. Warta, E. D. Dunlop. "Solar cell efficiency tables (version 39)." *Progress in Photovoltaics: Research and*

Applications, 2012, **20**: 12 – 20.

135. Gratzel, M. "Dye-sensitized solar cells." *Journal of Photochemistry and Photobiology C: Photochemistry Reviews*, 2003, **4**: 145 – 153.

136. Gratzel, M. "Solar Energy Conversion by Dye-Sensitized Photovoltaic Cells." *Inorganic Chemistry*, 2005, **44**: 6841 – 6851.

137. Gunes, S. H. Neugebauer, N. S. Sariciftci. "Conjugated Polymer-Based Organic Solar Cells." *Chemical Reviews*, 2007, **107**: 1324 – 1338.

138. Lin, Y., Y. Li, X. Zhan. "Small molecule semiconductors for high-efficiency organic photovoltaics." *Chemical Society Reviews*, 2012, **41**: 4245 – 4272.

139. Gundlach, D. J., Y. Y. Lin, T. N. Jackson, S. F. Nelson, D. G. Schlom. "Pentacene Organic Thin-Film Transistors – Molecular Ordering and Mobility." *IEEE Electron Device Letters*, 1997, **18**: 87 – 89.

140. Sakai, J., T. Tetsuya, T. Yamanari, Y. Yoshida, A. Fujii, M. Ozaki. "Pentacene:Fullerene Multilayer-Heterojunction Organic Photovoltaic Cells Fabricated by Alternating Evaporation Method." *Japanese Journal of Applied Physics*, 2010, **49**: 032301-1 – 7.

141. Li, Y., Y. Wu, P. Liu, Z. Prostran, S. Gardner, B. S. Ong. "Stable Solution-Processed High-Mobility Substituted Pentacene Semiconductors." *Chemistry of Materials*, 2007, **19**: 418 – 423.

142. Anthony, J. E., D. L. Eaton, S. R. Parkin. "A Road Map to Stable, Soluble, Easily Crystallized Pentacene Derivatives." *Organic Letters*, 2002, **4**: 15 – 18.

143. Hunter, C. A., J. K. M. Sanders. "The Nature of π-πInteractions." *Journal of the American Chemical Society*, 1990, **112**: 5525 – 5534.

144. Anthony, J. E., J. S. Brooks, D. L. Eaton, S. R. Parkin. "Functionalized Pentacene: Improved Electronic Properties from Control of Solid-State Order." *Journal of the American Chemical Society*, 2001, **123**: 9482 – 9483.

145. Chen, J., D. C. Martin, J. E. Anthony. "Morphology and molecular orientation of thin-film bis(triisopropylsilylethynyl) pentacene." *Materials Research Society*, 2007, **22**: 1701 – 1709.

146. Anthony, J. E. "Functionalized Acenes and Heteroacenes for Organic Electronics." *Chemical Reviews*, 2006, **106**: 5028 – 5048.

147. Park, S. K., T. N. Jackson, J. E. Anthony, D. A. Mourey. "High mobility solution processed 6,13-bis(triisopropyl-silylethynyl) pentacene organic thin film transistors." *Applied Physics Letters*, 2007, **91**: 063514-1 – 3.

148. Giri, G., E. Verploegen, S. C. B. Mannsfeld, S. Atahan-Evrenk, D. H. Kim, S. Y. Lee, H. A. Becerril, A. Aspuru-Guzik, M. F. Toney, Z. Bao. "Tuning charge transport in solution-sheared organic semiconductors using lattice strain." *Nature*, 2011, **480**: 504 – 508.

149. Becerril, H. A., M. E. Roberts, Z. Liu, J. Locklin, Z. Bao. "High-Performance Organic Thin-Film Transistors through Solution-Sheared Deposition of Small-Molecule Organic Semiconductors." *Advanced Materials*, 2008, **20**: 2588 – 2594.

CHAPTER 2

EFFECT OF UNIT CELL PARAMETERS ON THE ENERGY PROFILE OF 6,13-TIPS PENTACENE

The first part of this chapter will discuss some of the fundamental principles of Molecular Dynamics calculations used in this work. This will lead to a description of the procedure used to fit the missing parameters needed to complete the force field used to model 6,13-TIPS pentacene. The remainder of the chapter will then describe how this model was used to explore the energy landscape for 6,13-TIPS pentacene as we vary the unit cell parameters [a,b,γ]. These unit cell parameters control the geometry of the crystalline polymorphs of the system. Because of the Van der Waals forces, polymorphism (variations in crystal geometry) is common in organic semiconductors [1]. Since phase homogeneity is important for organic materials, undestanding polymorphism if vital to control phase mixing [1-3].

One of the first concepts to understand in relation to Molecular Dynamics (MD) is that of periodic boundary conditions [4-5]; for this study, a two-dimensional surface is modeled. Because only one unit cell is constructed in the simulations (which is not the case in experiment) and the effects of surrounding crystal structures need to be considered, periodic boundary conditions help take these considerations into account by modeling a continuous “mirror-image” structure that avoids edge effects [4]. Once the periodic boundary conditions, which are dependent upon the crystal geometry, are determined, the force field that best describes the system and

accurately reproduces experimental data needs to be established.

The force field used in all the calculations in this thesis is MM3, which has often been used in our group to describe organic semiconductor materials. The force field in a simulation is the blueprint for the interactions between atoms and molecules in the system; essentially it is the only major input to the MD simulation. The force field includes the atomic definitions, effective sizes, and partial charges; equilibrium bond lengths, angles, and dihedrals; Coulombic and van der Waals effects, etc.

Once all the force field parameters needed to describe the system under study are known, an algorithm is used to determine the energy of the system and to minimize this energy for a given set of processing conditions. These calculations search for the lowest-energy configuration of the system at the required specifications. An initial starting point that is fairly close to the equilibrium is essential so that the calculation can converge to an energy-minimized structure. This proved difficult at first since this system has not been extensively studied via computational methods. Chen *et al*. conducted a number of experimental studies on the 6,13-TIPS pentacene system [6]. This paper includes some computational results. However, their description of the computational model did not provide all of the required parameters to accurately describe the 6,13-TIPS pentacene system.

The organic semiconductor material, 6,13-TIPS pentacene, studied in this work was modeled using the Allinger *et al.* MM3 semi-empirical potential [7]. The MM3 method has been found to work well for representing the intermolecular forces in so-

called “small molecule” organic semiconductors [8-10]. MM3 is a semi-empirical model, with parameters fitted to reproduce certain properties of the chosen molecule. While the veracity of such models need to be validated against reference data (e.g., experimental data or *ab initio*-generated data), it is not possible to study polymorph formation in this molecule solely using an *ab initio* method. An *ab initio* representation of even a single unit cell of TIPS-pentacene molecules would have been a prohibitively expensive undertaking, hence the need to determine accurate semi-empirical models for TIPS-pentacene.

In order to model 6,13-TIPS pentacene molecules using the Allinger *et al.* MM3 potential [2], it is necessary to determine values for the parameters in the model. Many of these parameters are available using freely available Molecular Dynamics codes, such as TINKER [10]. However, not all the MM3 parameters needed to model this particular molecule were available in the literature; parameters were missing for the bond lengths, bond angles, and dihedral angles associated with an *sp*-carbon and silicon (the Si-C triple bond); see **Figure 2.1**.

In order to obtain these missing parameters, appropriate values for the equilibrium bond lengths, bond angles and dihedral angles were needed from an accurate source, in this case *ab initio* calculations. For this purpose, one molecule of 6,13-TIPS pentacene was constructed using the Avogadro software [8] and its structure was optimized in Gaussian09 [9] using the B3LYP hybrid functional and the 6-311++G(d,p) basis set. The equilibrium bond lengths, angles, and dihedrals determined from the Gaussian output as our reference data for the subsequent MM3

parameter fitting are listed in **Tables 2.1** and **2.2**: **Table 2.1** lists the equilibrium bond lengths and angles determined by this method and **Table 2.2** lists the dihedral angles. **Figure 2.1** illustrates the numbering scheme referenced in these Tables. Once the equilibrium parameters were obtained from the *ab initio* calculations, the next step involved determining force constants, again using *ab initio* techniques. To determine the stretching force constant, the bond length (C4-Si5 in **Figure 2.1**) was stretched and compressed in a series of small 0.1-Å steps, which yielded a plot of the change in configurational energy as the bond length was varied.

With all these *ab initio*-generated reference data in hand, we tackled fitting MM3 parameters to reproduce these data. The data shown in **Figure 2.1** were fitted against the equation for the MM3 potential for bond stretching used by Allinger *et al*. [7] (Eq. 2.1):

$$E_s = 71.94 * k_s * (l - l_0)^2 * [1 - 2.55*(l - l_0) + 3.79 * (l - l_0)^2]$$

[2.1]

In Eqn. 2.1, E_s is the configurational energy (kcal/mol); k_s is the stretching force constant (mdyne/Å); l and l_0 are the [varying] bond length (Å) and the equilibrium bond length (Å), respectively. **Figure 2.2a** provides a comparison between the single-point energy data calculated using Gaussian 09 as the bond length is varied and the corresponding MM3 results using Eqn. 2.1.

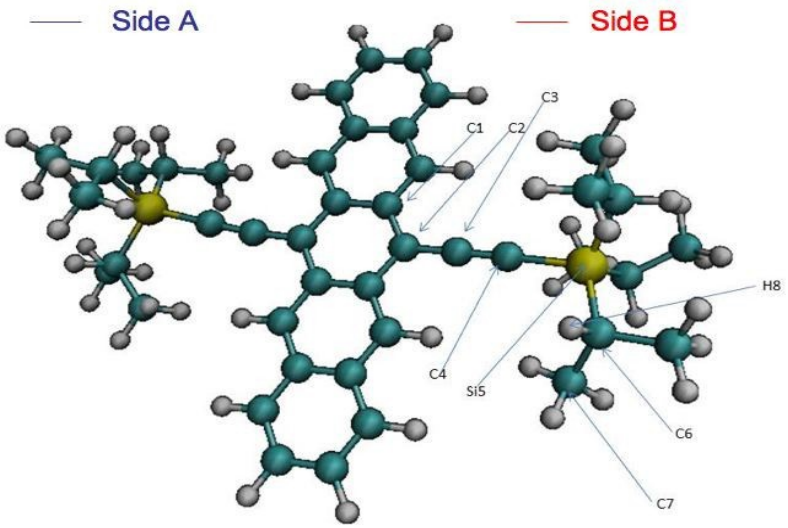

Figure 2.1. Numbering scheme for carbon (C), hydrogen (H), and silicon (SI) atoms in a TIPS-pentacene molecule, used to determine potential parameters.

Next, to calculate the bending force constant, the angles (C1-C2-C3, C3-C4-Si5, C4-Si5-C6 in **Figure 2.1**), were bent in 1° increments and the resulting change in configurational energy was plotted against varying values for the bond angles. The rotations were completed using quaternions, which are three-dimensional rotation matrices [11]. The data were then fitted against the relevant equation for the MM3 potential for angle bending [7] shown in Eqn. 2.2:

$$E_\theta = 0.021914 * k_\theta * (\theta - \theta_0)^2 * [1 - 0.014 * (\theta - \theta_0) + 5.6*10^{-5} * (\theta - \theta_0)^2 - 7*10^{-7} * (\theta - \theta_0)^3 + 2.2*10^{-8} * (\theta - \theta_0)^4] \quad [2.2]$$

In Eqn. 2.2, E_θ is the configurational energy (kcal/mol); k_θ is the bending force constant (mdyne Å/rad^2); and θ and θ_0 are the varying bond angles (°) and equilibrium bond angle (°) respectively. In a similar manner to the bond-stretching fitting procedure above, **Figure 2.2b** provides a plot of the single-point energy data from Gaussian 09 for the C3-C4-Si5 angle in comparison to the MM3 results predicted using Eqn. 2.2.

Values for the Fourier coefficients for the dihedral angles containing an *sp*-carbon and silicon were taken from those containing an s*p*^{2}-carbon and silicon. The rationale for this is that the side groups are fairly rigid, regardless of whether they contain a carbon-carbon double bond or a triple bond.

A computational description of a unit cell containing four TIPS-Pn molecules was constructed using values for [a, b, γ] that represent the bulk single crystal for the equilibrium polymorph as determined by Anthony *et al.* [12]: a-axis = 7.75 Å; b-axis

= 7.56 Å; and γ = 96.4°. The c-axis was set to 1000 Å in order to simulate a two-dimensional structure. The energy of this unit cell was then minimized in TINKER and was used as the reference point for the energy difference quoted in all subsequent calculations.

To determine the energy landscape as the [a,b,γ] parameters were varied, the effect of varying these three parameters was explored in the following broad ranges: 7.2 – 8.1 Å for the a-axis; 7.2 – 9.36 Å for the b-axis; and 72 – 116° for γ. Each choice of [a,b,γ] was submitted to an energy minimization calculation within TINKER and then the reference equilibrium energy was subtracted from the resulting configurational energy relevant to that [a,b,γ] choice. This produces the values of ΔE shown in **Table 2.3**.

Table 2.1. MM3 parameters for bond lengths and angles for the *sp*-carbon and silicon atoms in 6,13-TIPS Pentacene.

Bond	**k_s (mdyne/Å)**	**l_0 (Å)**
C4-Si5	2.782	1.85
Angle	**k_θ (mdyne/Å rad^2)**	**θ_0 (°)**
C1-C2-C3	1.52	119.81
C3-C4-Si5	0.1918	179.39
C4-Si5-C6	0.9037	108.69

Table 2.2. MM3 parameters for dihedral angles for the *sp*-carbon and silicon atoms in 6,13-TIPS Pentacene

Dihedral	**V_1 (kcal/mol)**	**ω_0 (°)**	**V_2 (kcal/mol)**	**ω_0 (°)**	**V_3 (kcal/mol)**	**ω_0 (°)**
C2-C3-C4-Si5	0	0	6.45	21.69	0	0
C3-C4-Si5-C6	-0.3	0	0	229.36	0	0
C4-Si5-C6-C7	0	0	0	45.36	0.167	0
C4-Si5-C6-H8	0	0	0	182.27	0.117	0

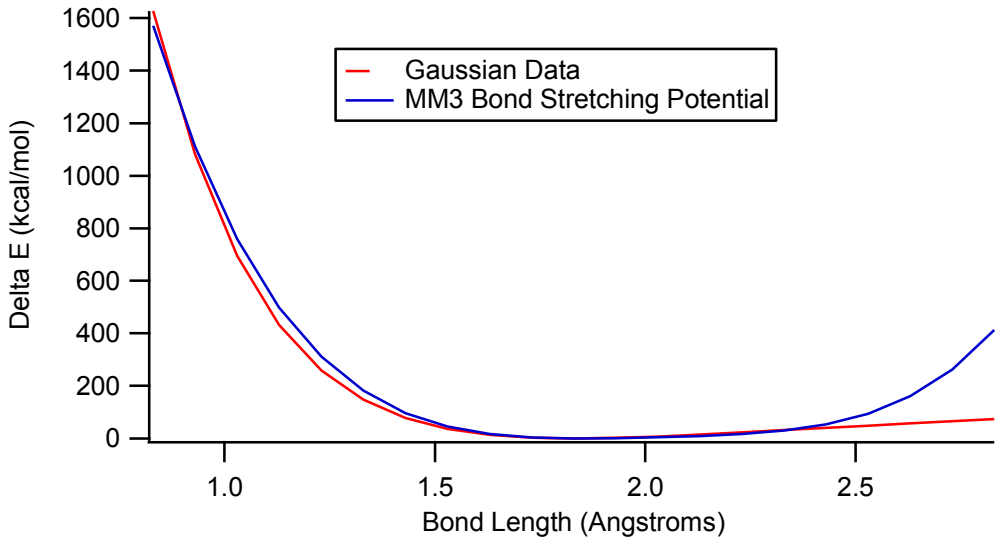

Figure 2.2a. Energy of bond stretching in the C4-Si5 as a function of change in the C4-Si5 bond length. Results for Gaussian 09 data are shown as a dashed red line. The result of fitting the Gaussian09 data to the MM3 potential using Eqn. 1 are shown as a solid blue line.

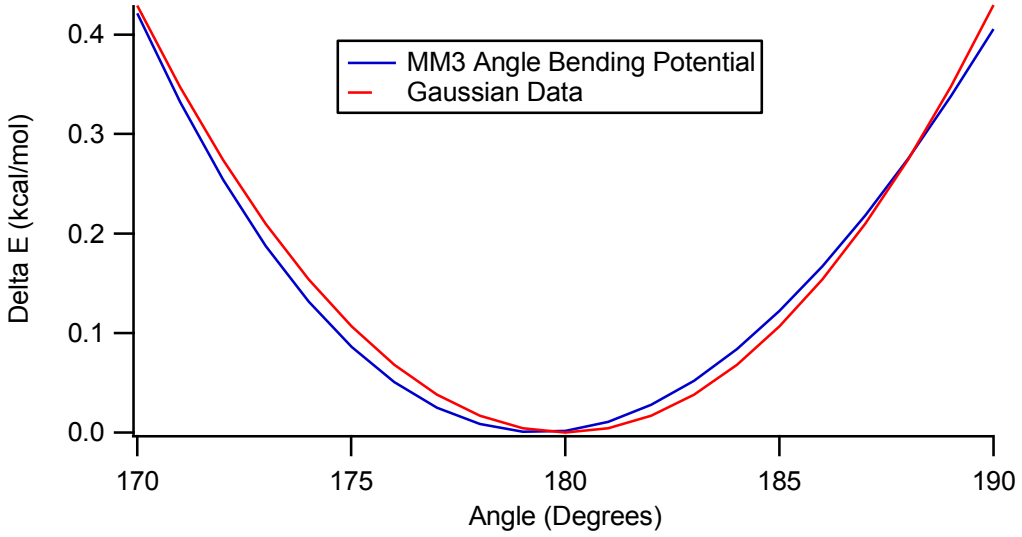

Figure 2.2b. Energy of bond bending in the C3-C4-Si5 bond as a function of change in the C3-C4-Si5 bond angle. Results for Gaussian 09 data are shown as a dashed red line. The result of fitting the Gaussian 09 data to the MM3 potential using Eqn. 2 are shown as a solid blue line.

Scanning [a, b, γ] space allowed the identification of a set of the lowest energy states within the computed energy landscape. **Table 2.3** compares the computationally derived predictions of [a, b, γ] against experimental values for the five lowest-energy configurations of the unit cell. ΔE_{offset} is the difference in ΔE for the polymorphs using the ΔE of polymorph I as the baseline. It was estimated that the uncertainty in the energies is between 0.01 and 0.02 eV. Thus with some confidence, the three major families of polymorphs (I, II, III) can be distinguished, but distinguishing the polymorphs within each family is more challenging. This prompted the decision to simply report the five lowest energies and match them as being synonymous with the polymorphs found in experiments.

As can be seen in **Table 2.3**, the computational values for all of the polymorphs fit well against the experimental data: differences in 'a' and 'b' are around 0.1-0.2 Å (2-3%) and those in γ are, at worst, <4° (<5%). The range of the relative energies (ΔE) is practically identical for all five polymorphs, showing the relative flatness of the energy landscape in which the polymorphs are found. Despite the flatness of the energy landscape, the predicted relative energies of three major polymorphs match qualitatively with the experimental data. Given that finding the crystal structure for a molecule like TIPS-pentacene is particularly challenging due to the conformational flexibility of the molecule, the degree of reproduction of the experimental data is very encouraging.

Figure 2.3 shows the energy landscape that was calculated to obtain the results in Table 4. This 4-dimensional space is shown by plotting the change in energy (as in Table 4), ΔE, as two of the [a,b,γ] parameters are varied, while keeping the third of these parameters constant. It was particularly interesting to investigate whether the minimum is isotropic across all three parameters; that is, is the minimum "bowl" shaped or does it resemble a valley floor? It can be seen that, in general, the energy landscape is not isotropic. For instance, **Figs. 2.3a-b** show the energy minimum for polymorph I, in which there is no symmetry about either the a- or b-axis and some symmetry about γ. For polymorph II, **Figs. 2.3c-d** again see no symmetry is seen about the a-axis and slight symmetry is noticed about the b-axis. For polymorph III, **Figs. 2.3e-f** shows that there is no symmetry about either the a- or b-axis. Overall, the topology of the energy landscape is such that it is less sensitive to changes in the a- and b-axes than changes in γ. To repeat the metaphor used above, the energy profile is not an isotropic bowl shape but a valley floor in which changes in a and b are "sloppy," [13] but changes in γ are stiff. This computational finding is consistent with experimental data: that γ is the major unit cell parameter distinguishing three families of polymorphs.

Table 2.3. Comparison of Experimental and Calculated Parameters for the Five Lowest Energy State and Polymorph Identification

Polymorph	**a (Å)**	**b (Å)**	**γ (°)**	**ΔE (eV)**	**ΔE_{offset} (meV)**
I (expt.)	7.68	7.77	81.46	-	-
I (calc.) (expt. – calc.)	7.56 (0.1)	8.00 (-0.2)	80.0 (1.5)	-1.217	0
Ib (expt.)	7.67	7.91	80.25	-	-
Ib (calc.) (expt. – calc.)	7.56 (0.1)	8.10 (-0.2)	80.0 (0.2)	-1.203	14
II (expt.)	7.48	8.50	71.29	-	-
II (calc.) (expt. – calc.)	7.75 (-0.3)	8.40 (0.1)	68.0 (3.3)	-1.156	61
IIb (expt.)	7.57	8.59	71.67	-	-
IIb (calc.) (expt. – calc.)	7.76 (-0.2)	8.64 (-0.05)	68.0 (3.7)	-1.150	67
III (expt.)	7.56	9.02	65.23	-	-
III (calc.) (expt. – calc.)	7.75 (-0.2)	8.64 (0.4)	63.9 (1.3)	-1.134	83

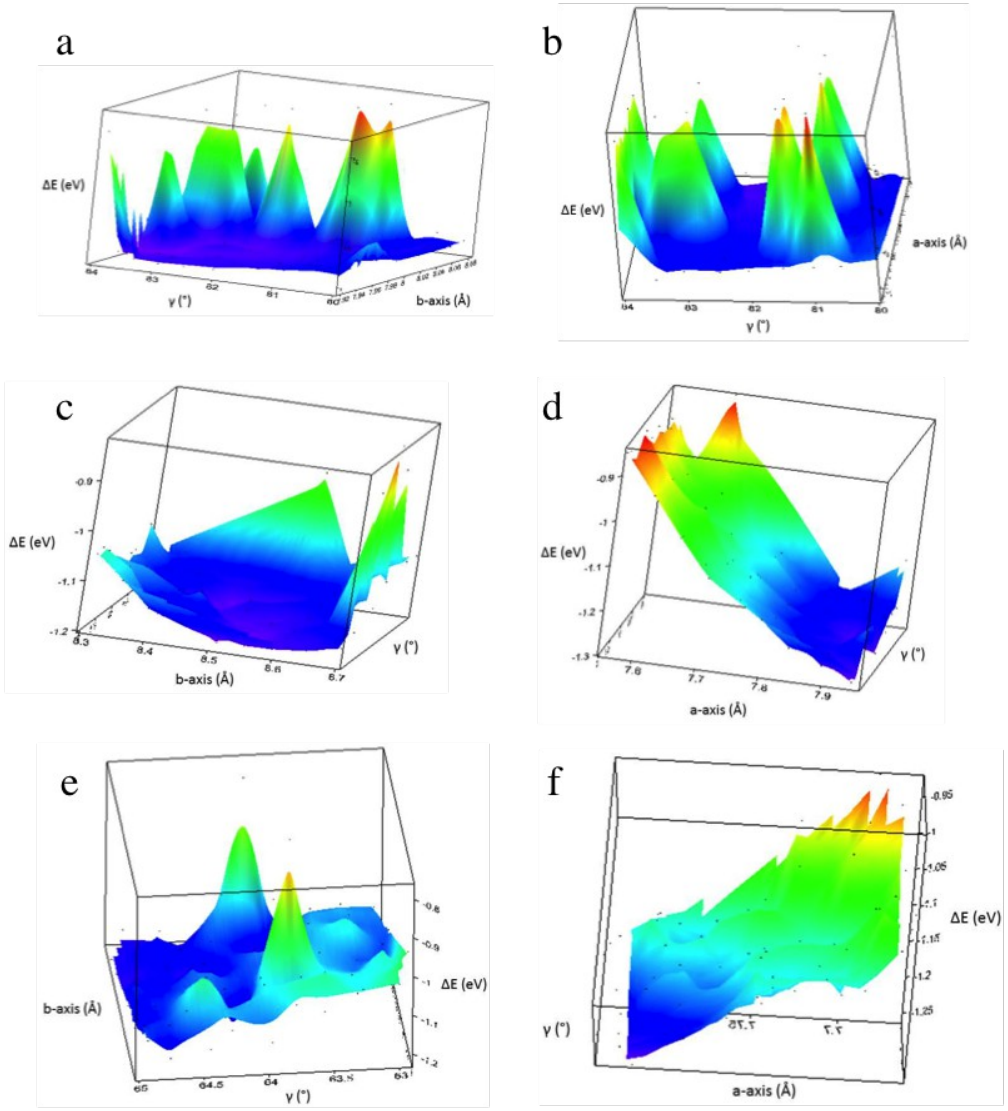

Figure 2.3. Energy landscapes for each of the three polymorphs to determine their relative insensitivities to changes in a,b, and ɣ parameters. **Fig. 2.3a-b**: Polymorph I. **Fig. 2.3c-d**: Polymorph II. **Fig. 2.3e-f**: Polymorph III.

The structural consequences of making changes to [a,b,γ] were investigated on the disposition of the acene backbone, the rotation of the methyl groups and the silyl-ethynyl angle in the TIPS functional group, as described in the following sub-sections.

A small amount of bending in the acene backbone was observed (**Fig. 2.4**) and some twisting taking place as [a,b,γ] were varied. This was done by holding one of the parameters constant at the calculated equilibrium value (*i.e.,* b=8.0 Å) and varying a and γ. In **Fig. 2.5a**, each point is an average of the changes in the acene angle for all values of a at that particular value for γ. Angular changes of up to 4.5° can be observed when γ is varied; whereas changes in either the a- or b-axis at constant γ produce backbone bending of less than 2°. This reinforces the shape of the energy landscapes observed in **Figure 2.3** in which it was found that changing the a- and b-axes alters the energy landscape less than changes in γ. **Figs. 2.5 a-b** also show that structural changes in the two sides of the acene backbone, which are called side A and B, oppose each other, inducing strain into the backbone. This strain is minimized when γ reaches a value in the range ~80°, which encloses the region in which both polymorphs I and Ib occur (80°). At constant γ of 80° (**Fig. 2.5c**), the opposition of sides A and B again work against each other, but a minimum distortion in the angle of the acene backbone (~0.6°) occurs at about 7.6 Å (the location of the calculated structures for polymorph I) and at about 7.8 Å, which corresponds to polymorphs II and III.

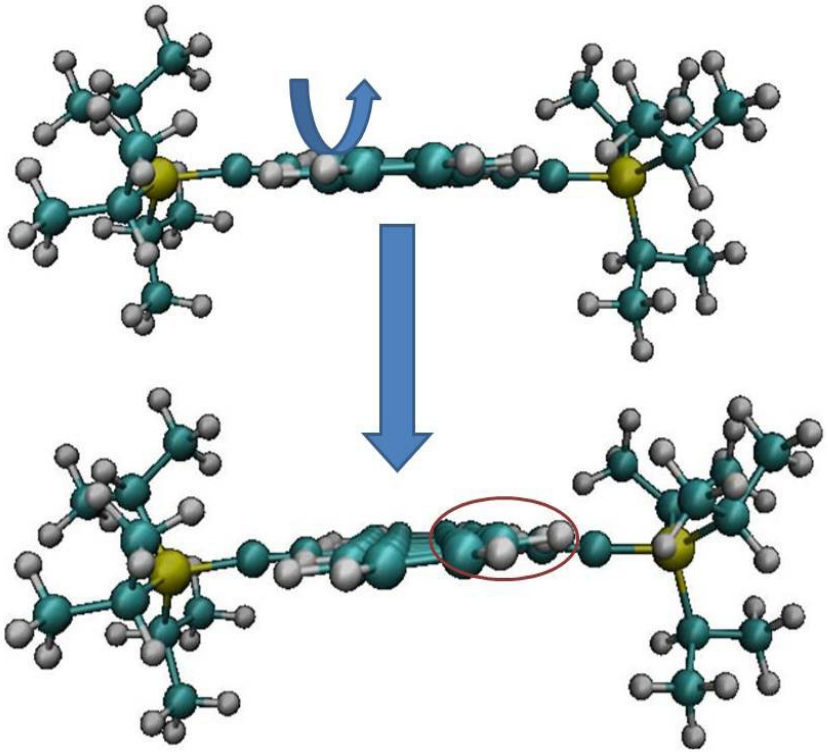

Figure 2.4. Observation of bending (top) and twisting (bottom) of the acene backbone.

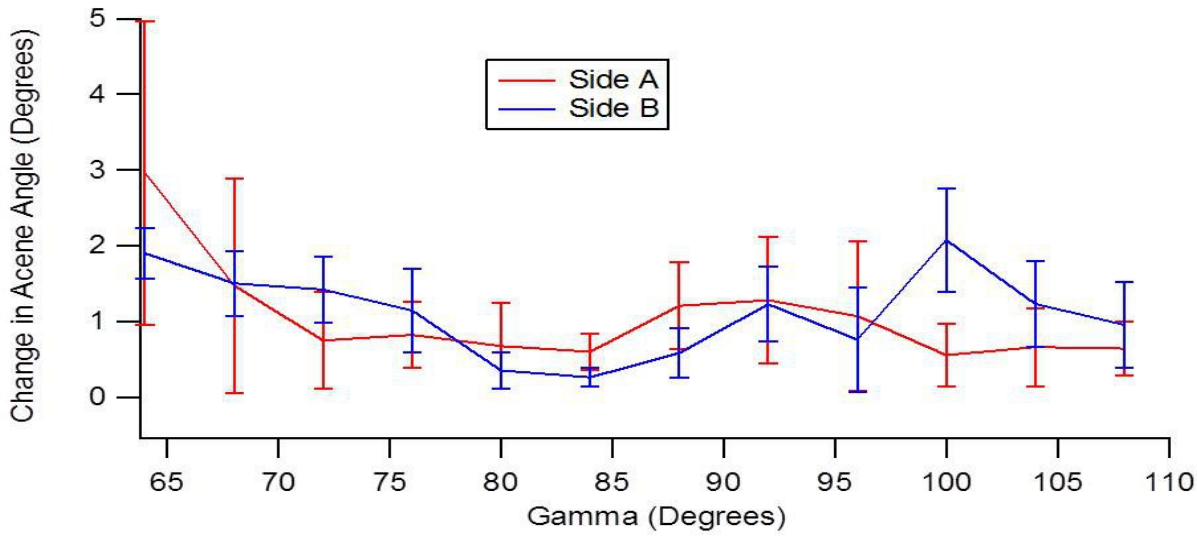

Fig. 2.5a. Changes in acene angle with respect to γ at constant b=8 Å.

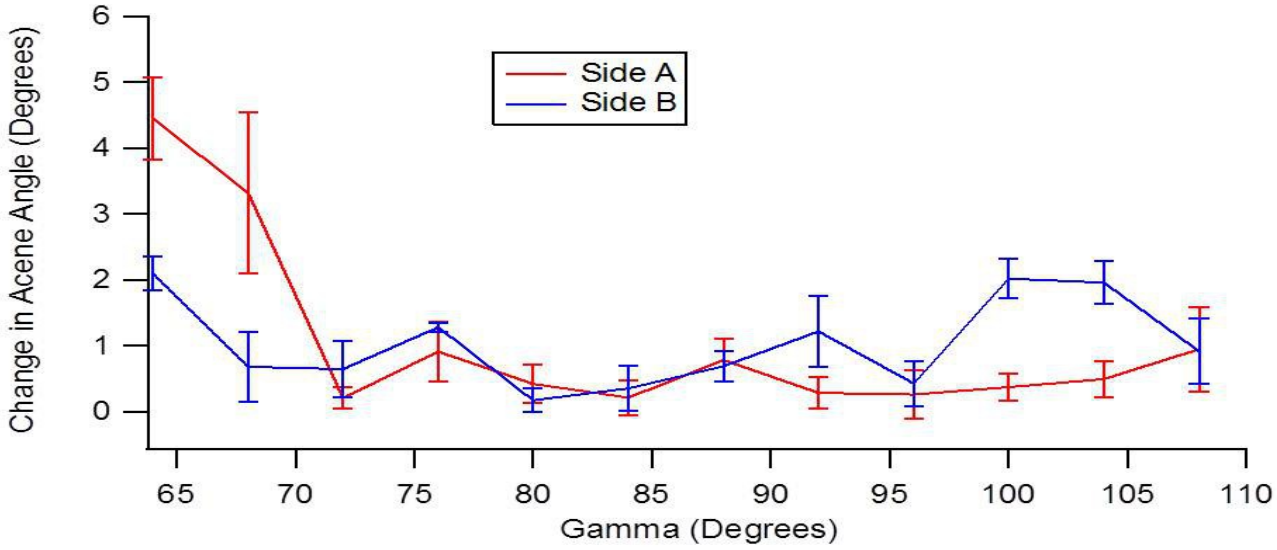

Fig. 2.5b. Changes in acene angle with respect to γ at constant a=7.56 Å.

Fig. 2.5c. Changes in acene angle with respect to the a-axis at constant γ=80°.

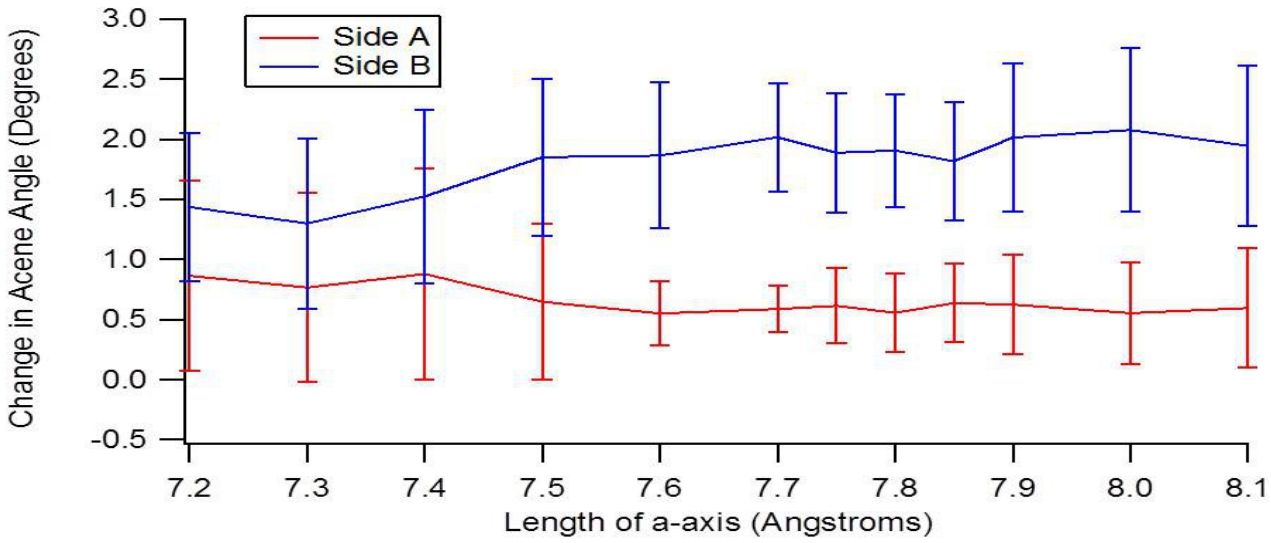

The effect on the strain in the molecule as the methyl groups attached to the silicon atom is allowed to rotate was considered, as shown in **Figure 2.6**. The hypothesis was that, as the methyl groups comprising the TIPS group "ratcheted" around, they would cause a conformational strain that would be manifested in a rise in energy. It is believed that this rotation is the origin of the acene backbone twist and bending observed in subsection (a) above. In a similar fashion to **Fig. 2.5**, **Figure 2.7** shows how the energy varies as two of the [a,b,γ] parameters were changed while keeping the third constant. Minima are seen in the vicinity of γ values in the region of 76-80° and 92-96° in **Figs. 2.7a-b**, closest to polymorphs I and II. The γ value of ~64° corresponding to polymorph III in the calculations produces a particularly strained angle up to 4° different from that of the experimental value for the bulk. For data at constant γ, **Fig. 2.7c** shows the lowest distortion of the methyl angle from the equilibrium value in the region of 8.0 (characteristic of polymorph I) and 7.3 (which is not characteristic of any of the polymorphs).

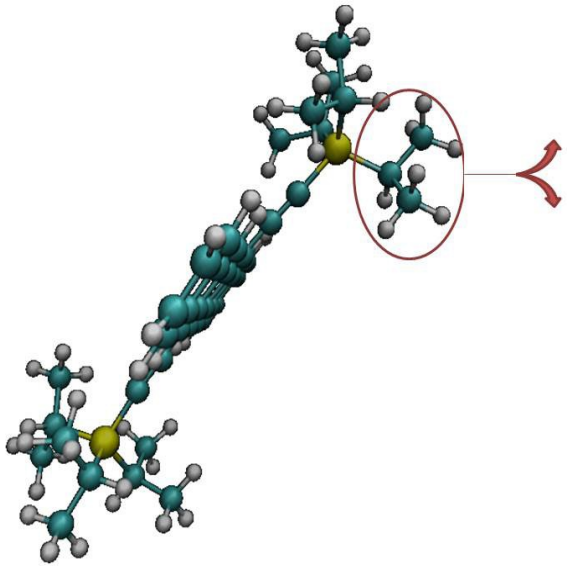

Figure 2.6. Illustration of the methyl groups attached to the Si atom of the TIPS group, whose rotational movement we monitored.

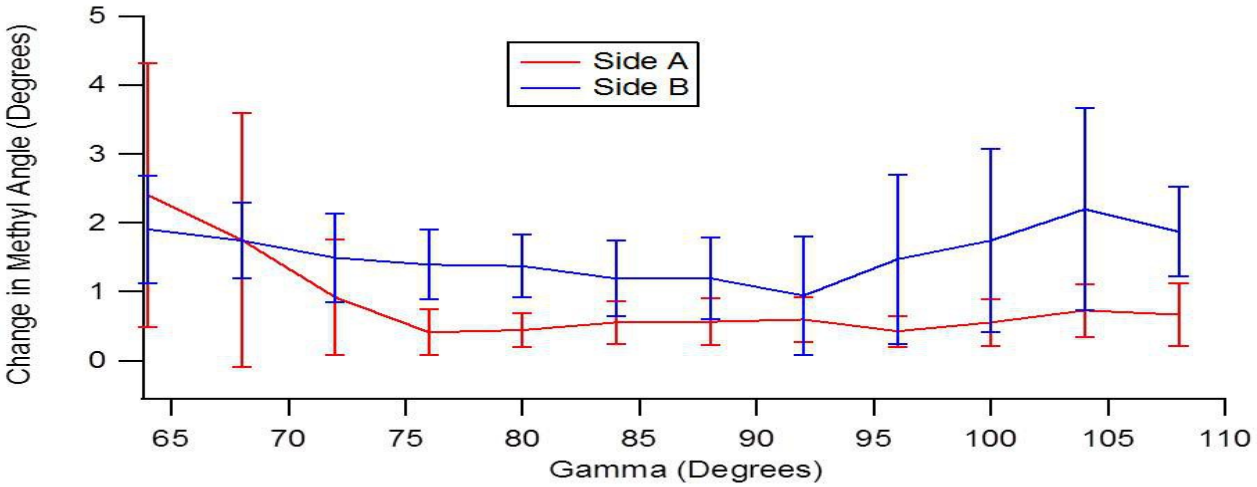

Fig. 2.7a. Changes in methyl angle with respect to γ at constant b=8 Å.

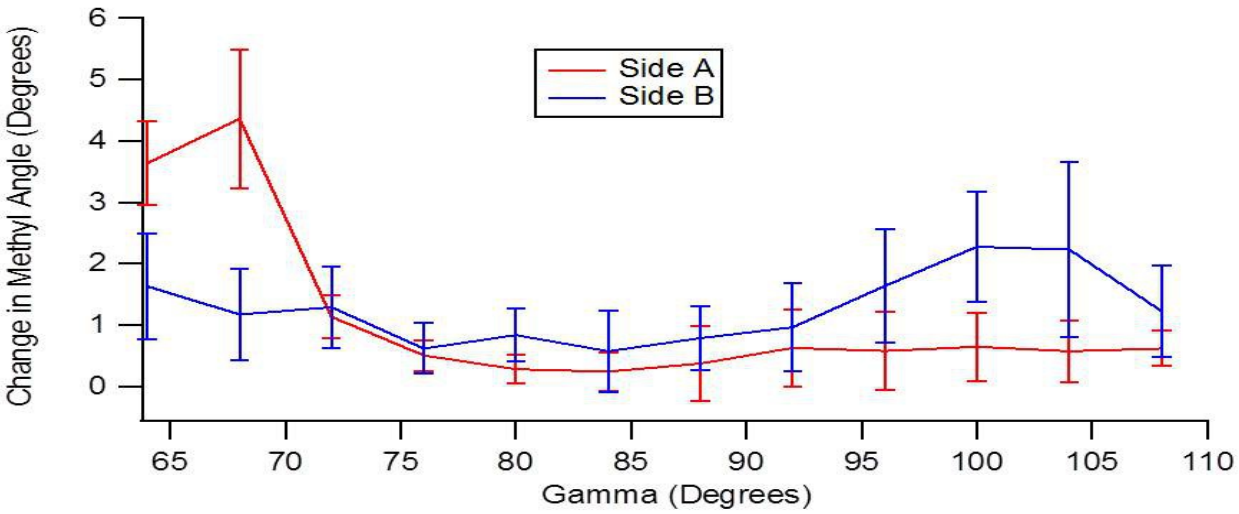

Fig. 2.7b. Changes in methyl angle with respect to γ at constant a=7.56 Å.

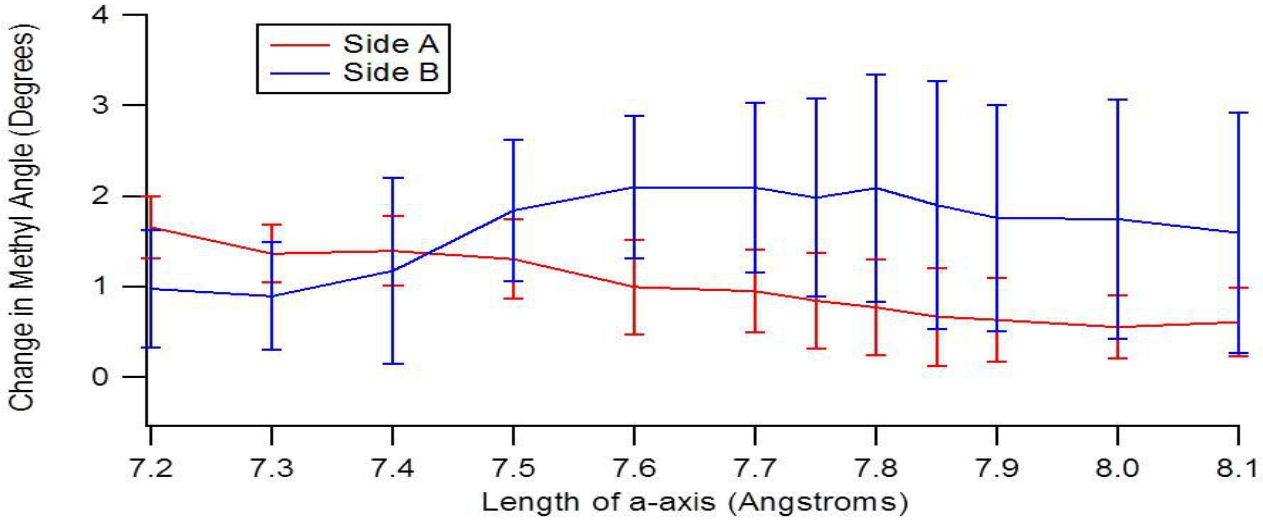

Figure 2.7c. Changes in methyl angle with respect to a at constant γ=80°.

The origin of the degree of bending and twisting of the acene backbone observed above could also lie in the tendency of the bulky TIPS group to "wag" up and down relative to the plane of the acene backbone, that is, changes in the silyl-ethynyl angle, as shown in **Figure 2.8**. In a similar manner to the preceding subsections, differences in the silyl-ethynyl angle were observed as two of the three [a,b,γ] parameters were varied. **Figures 2.9a-b** show differences in this angle from the equilibrium structure when a and b, respectively, are held constant. It can be seen that relatively large changes of up to nearly 8° are possible. This causes a larger distortion than either the rotation of the methyl groups in the TIPS moiety or the bending of the backbone in absolute terms. Minima occur at 68° (closest to polymorph II), 84° (closest to polymorph I) and 100° (close to polymorph I) with the least strain at 84°.

The two sides of the molecule oppose each other at low values of γ; for constant a or b, they converge around 84° (close to polymorphs I and Ib). **Fig. 2.9c** shows the difference in the silyl-ethynyl angle for constant γ; here it can be seen that the strain in this "wag" angle reduces as the value of a or b increases. It is lowest around 8.0 and 8.1, close to values for polymorphs I.

Taking the results of all these three structural changes together, *i.e.,* changes in the angular disposition of the acene backbone to bend or twist, the wagging of the silyl-ethynyl groups, and the rotation of the methyl groups, it is noted that the resultant strain in the molecules is minimized at [a,b,γ] values consistent with the energy minima previously calculated and hence with the major polymorphs (**Table 2.3)**.

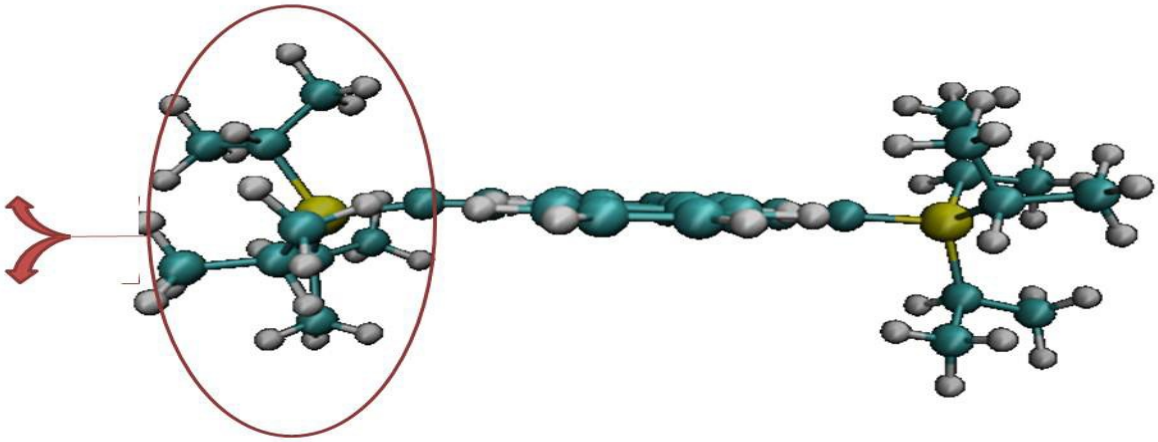

Figure 2.8. Identification of the silyl-ethynyl angle, circled in brown, whose tendency to wag up and down (as indicated by the arrows) was studied as we vary the unit cell parameters.

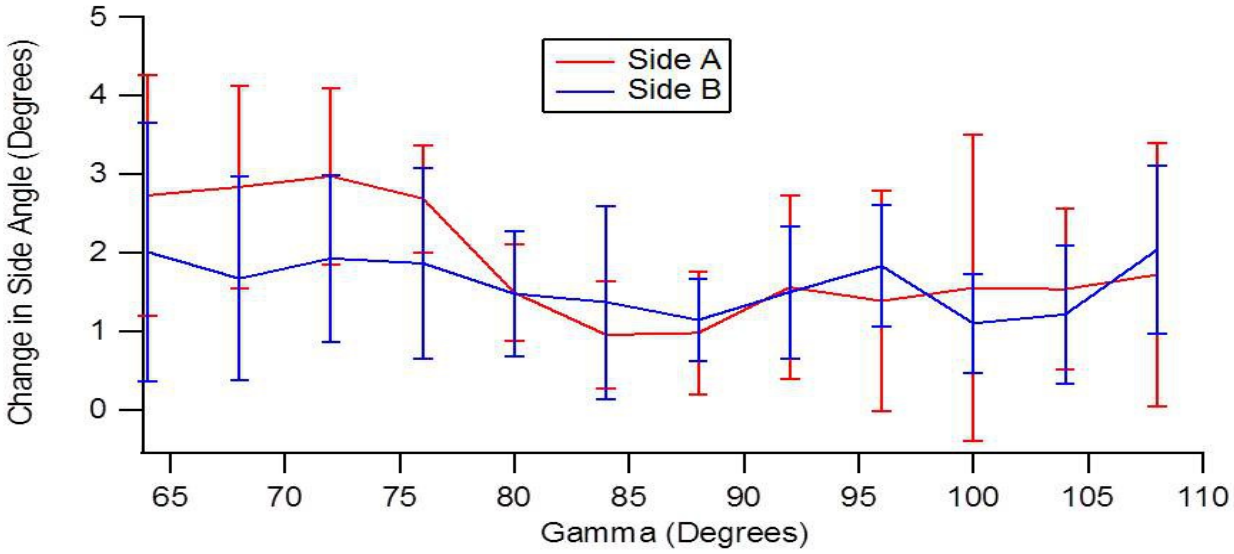

Fig. 2.9a. Changes in the angle that the silyl-ethynyl angle makes with the acene backbone (zero degrees implying c-planar with the backbone) with respect to γ at constant b=8 Å.

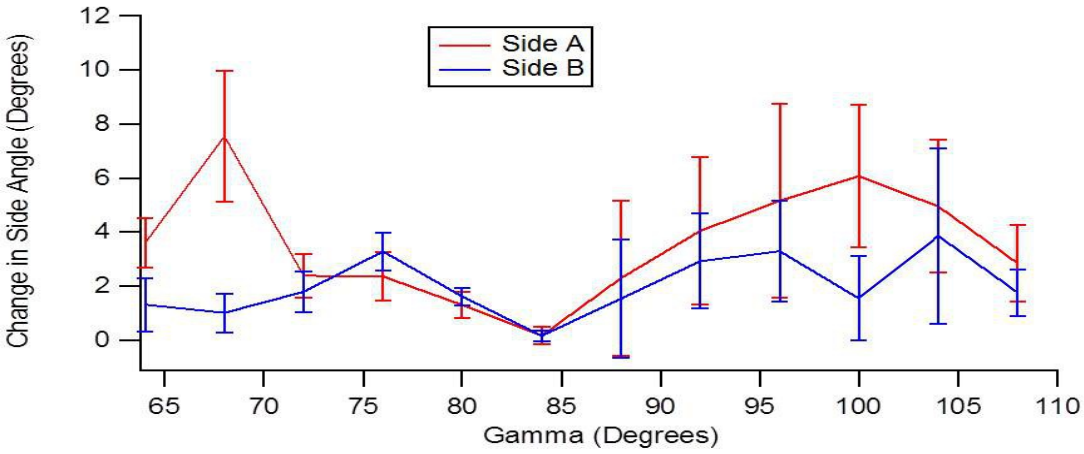

Fig. 2.9b. Changes in the angle that the silyl-ethynyl angle makes with the acene backbone (zero degrees implying c-planar with the backbone) with respect to γ at constant a=7.56 Å.

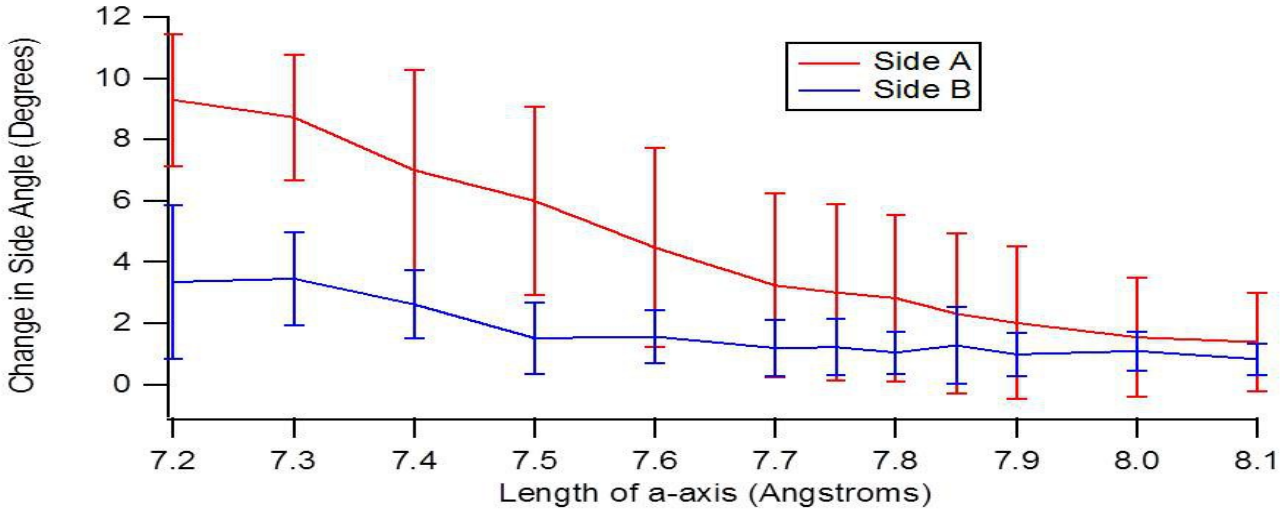

Figure 9c. Changes in the angle that the silyl-ethynyl angle makes with the acene backbone (zero degrees implying c-planar with the backbone) with respect to a at constant γ=80°.

REFERENCES

1. Brillante, A., I. Bilotti, R. G. D. Valle, E. Venuti, A. Girlando. "Probing polymorphs of organic semiconductors by lattic phonon Raman microscopy." *CrystEngComm*, 2008, **10**: 937 – 946.

2. Brillante, A., I. Bilotti, R. G. D. Valle, E. Venuti, M. Masino, A. Girlando. "Characterization of Phase Purity in Organic Semiconductors by Lattice-Phonon Confocal Raman Mapping: Application to Pentacene." *Advanced Materials*, 2005, **17**: 2549 – 2553.

3. Brillante, A., I. Bilotti, C. Albonetti, J-F. Moulin, P. Stoliar, F. Biscarini, D. M. de Leeuw. "Confocal Raman Spectroscopy of α-Sexithiophene: From Bulk Crystals to Field-Effect Transistors." *Advanced Functional Materials*, 2007, **17**: 3119 – 3127.

4. Allen, M. P., D. J. Tildesley. *Computer Simulation of Liquids.* Oxford: Oxford University Press, 1987.

5. Frenkel, D., B. Smit. *Understanding Molecular Simulation: From Algorithms to Applicatoins*. Waltham: Academic Press, 2001.

6. Chen, J., J. Anthony, D. C. Martin. "Thermally Induced Solid-State Phase Transition of Bis(triisopropylsilylethynyl) Pentacene Crystals." *Journal of Physical Chemistry B*, 2006, **110**: 16397 – 16403.

7. Allinger, N. L.; Yuh, Y. H.; Lii, J. H. *Journal of the American Chemical Society* **1989**, *111*, 8551.

8. http://avogadro.openmolecules.net/wiki/Main_Page

9. http://gaussian.com/

10. http://dasher.wustl.edu/tinker/

11. Hanson, A. J. *Visualizing Quaternions*. Amsterdam: Elsevier, 2006.

12. Anthony, J. E.; Brooks, J. S.; Eaton, D. L.; Parkin, S. R. *Journal of the American Chemical Society* **2001**, *123*, 9482.

13. Machta, B. B.; Chachra, R.; Transtrum, M. K.; Sethna, J. P. *Science* **2013**, *342*, 604.

CHAPTER 3

EFFECT OF SOLVENT SIZE ON THE ENERGY PROFILE OF 6,13-TIPS PENTACENE

Molecular simulation techniques were used to determine the effect of both solvent molecule size (in terms of the molar volume) on the energetic preference for a particular polymorph of the TIPS pentacene as well as the local impact of a solvent molecule on the bend of the acene backbone on proximal TIPS pentacene molecules.

As stated above, the goal of this study was to investigate the effect of residual solvent on the selection of the most energetically favored polymorph. The reason for this study was the experimental observation that their choice of solvent affected the polymorph that was exhibited. The solution-shearing process is a complex combination of shearing, crystal nucleation and growth, and solvent evaporation. Our approach was to take one piece of this process, essentially the last stages of crystal formation, and study the interaction of the TIPS pentacene omlecules in the unit cell with a nearby solvent molecule. The intent was to determine how the unit cell dimensions [a,b,γ] respond to the presence of this solvent molecule in order to minimize the energy of the system. A secondary goal was to determine the response of the molecular configurtion to the presence of the solvent molecule. Here, we were looking at any extent of backbone bending, etc., as in the previous study of TIPS pentacene polymorphism described in the preceding chapter.

In order to set up this study, we built one molecule of 6,13-TIPS pentacene using Avogadro [1] and optimized its configuration in Gaussian09 [2] using the B3LYP hybrid functional and the 6-311++G(d,p) basis set. The resulting model, in terms of the detailed structural coordinates of the atomic constituents of the molecule, was then minimized in the well-known Molecular Dynamics code, TINKER[3], with periodic boundary conditions of 1000 Å in each direction. The resulting structure was used to build a unit cell containing four molecules of 6,13-TIPS pentacene *via* TINKER's built-in "crystal" program. The parameters used to build the unit cell were those observed experimentally[4] as the equilibrium polymorph. That is the parameters are: a-axis = 7.75 Å; b-axis = 7.56 Å; and $\gamma = 96.4°$. The c-axis was set to 1000 Å in order to simulate a two-dimensional structure. The energy of this unit cell was then minimized in TINKER and was used as the baseline for the change in energy calculations.

The commonly used solvents studied experimentally cover a range of molecular sizes and other important molecular characteristics, such as multiple moments. In this study, we were interested in separating the effect of solvent size on the energy profile of 6,13-TIPS pentacene from any potentially countermanding polarity effects. To that effect, a single spherical (non-polar) Lennard-Jones (LJ) atom of varying radius was placed between two of the molecules of the unit cell, as shown in **Figure 3.1.** The radius of the effective LJ atom determined to be appropriate for each solvent was determined by assuming a spherical shape for the solvent molecule and using its experimentally determined molar volume as a guide.

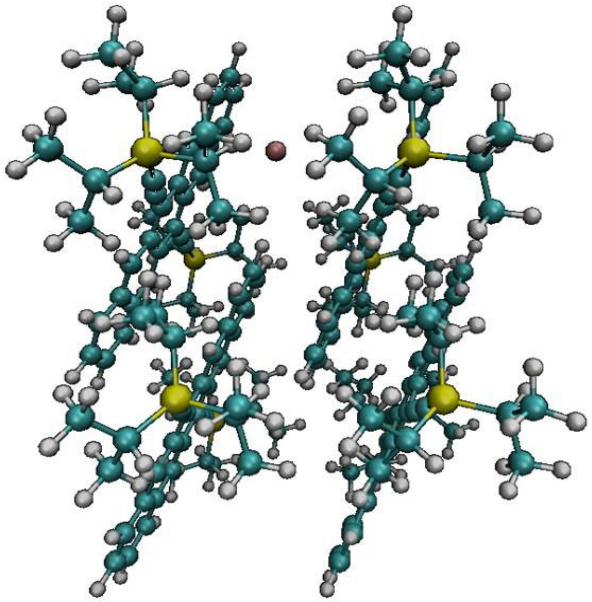

Figure 3.1. 6,13-TIPS Pentacene unit cell showing position of inserted Lennard-Jones atom (brown).

The energy of the system, TIPS pentacene molecules and interspersed LJ atom, was then allowed to minimize. For the results reported below, the energy of the equilibrium unit cell without the LJ 'solvent' molecule present was subtracted from the energy of each of the minimized unit cells to determine the energy difference to the system resulting from its inclusion as a function of the radius of the inserted LJ atom.

The radius of the LJ atom was varied from 3.18 to 3.94 Å in order to cover solvents ranging from tetrahydrofuran (equivalent LJ radius of 3.18 Å) to tetralin (equivalent LJ radius of 3.94 Å) that are of interest in the experimental studies. **Table 3.1** provides a list of the solvents used, their experimental molar volumes, and their resulting radii if represented as a LJ sphere.

To determine how the presence of the Lennard-Jones atom affects the energy profile of the crystal structure, the unit cell parameters were varied over the following ranges: 7.2 – 8.1 Å along the a-axis, 7.2 – 9.36 Å along the b-axis, and 72 – 116° for γ.

Table 3.2 lists the solvents in order of increasing Lennard-Jones radii, the change in energy caused by the presence of the LJ atom (shown as ΔE_{equil} in eV) and their preferred [a, b, γ] parameters corresponding to their lowest-energy configuration.

Looking at the values of ΔE_{equil} in Table S1, it is clear that the energy is most favorable (most negative) for the smallest solvents and that there is a consistent trend of decreasing configurational stability with increasing solvent radius.

Table 3.1. Table of Solvents, Molar Volumes, and equivalent Lennard-Jones Radii

Solvent	**Molar Volume (Å^3/mol)**	**Effective Lennard-Jones Radius (Å)**
Tetrahydrofuran (THF)	134.7	3.18
1,4-Dioxane	141.7	3.23
Benzene	148.0	3.28
Chlorobenzene	168.4	3.43
Toluene	176.6	3.48
o-Dichlorobenzene	187.8	3.55
m-Xylene	205.1	3.66
Tetralin	226.4	3.78
Mesitylene	231.2	3.81
Decalin	256.3	3.94

The average of all the changes in energy over the entire range of [a,b,γ] parameters that we studied was calculated as the radius of the LJ atom "solvent" molecule is changed (see **Figure 3.2**). As such, *each* data point in **Figure 3.2** corresponds to the aggregate of 432 values of the energy from different [a,b,γ] combinations. As might be expected, this figure shows a linear tendency in the change in energy with the solvent radius. The range of solvents studied cover a significant change in ΔE, a range of about 0.5 eV, which is surely sufficient to affect the behavior of the crystallizing TIPS pentacene molecules. The error bars in **Figure 3.2** reflect the median absolute deviation (MAD).

Figure 3.2b provides a box plot of values of ΔE for the solvents; it shows the median, upper and lower quartiles, and the extent of outliers (outliers are the red crosses) for each case. As can be seen from the graph, there are few outliers relative to the total number of data points.

Table 3.2. Effective LJ spheres representative of "Solvent" atoms and their effect on preferred crystal structure parameters

LJ "Solvent"	**LJ radius (Å)**	**ΔE_{equil} (eV)**	**a-axis (Å)**	**b-axis (Å)**	**γ (°)**
THF	3.18	-2.14	8.29	7.80	75.16
1,4-Dioxane	3.23	-1.96	8.04	7.79	77.30
Benzene	3.28	-1.97	7.95	7.74	75.46
Chlorobenzene	3.43	-1.87	8.28	7.79	74.33
Toluene	3.48	-1.85	7.95	7.75	75.32
o-Dichlorobenzene	3.55	-1.79	8.00	7.75	75.60
m-Xylene	3.66	-1.64	8.24	7.97	76.10
Tetralin	3.78	-1.57	8.26	7.92	72.52
Mesitylene	3.81	-1.61	7.45	7.97	73.87
Decalin	3.94	-1.32	7.79	7.54	70.87

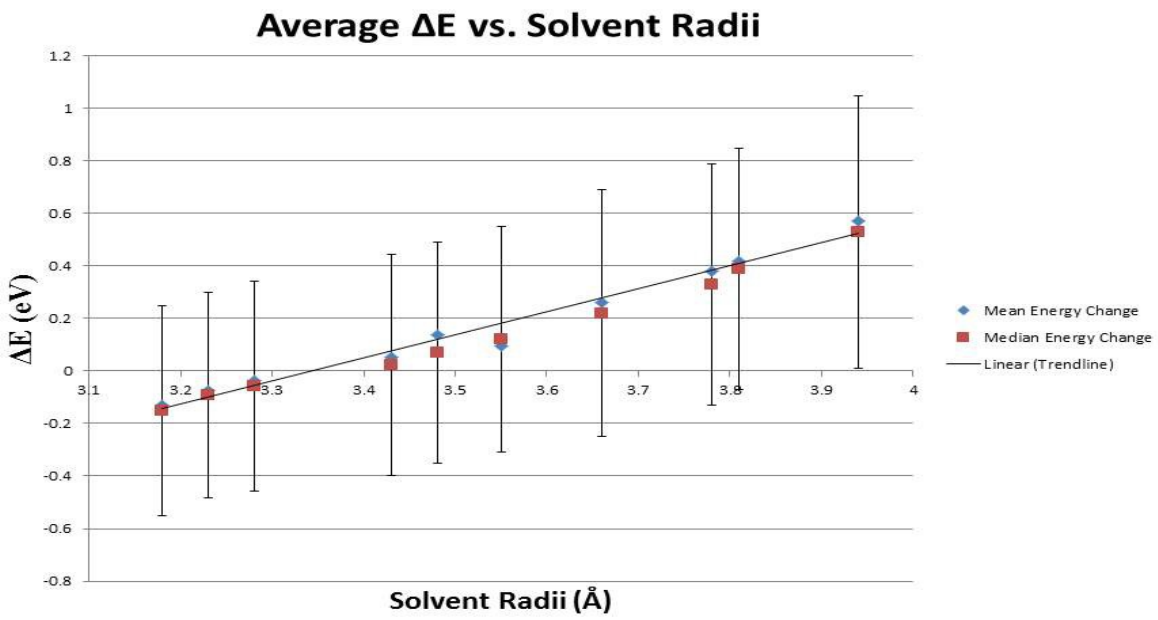

Figure 3.2a. Average change in the energy of a TIPS pentacene unit cell as the radius of the inserted LJ atom is increased. Mean energy change shown as blue dots; median energy change shown as red dots. A linear fit to the data is shown as a solid black line. Error bars are provided in terms of the median absolute deviation.

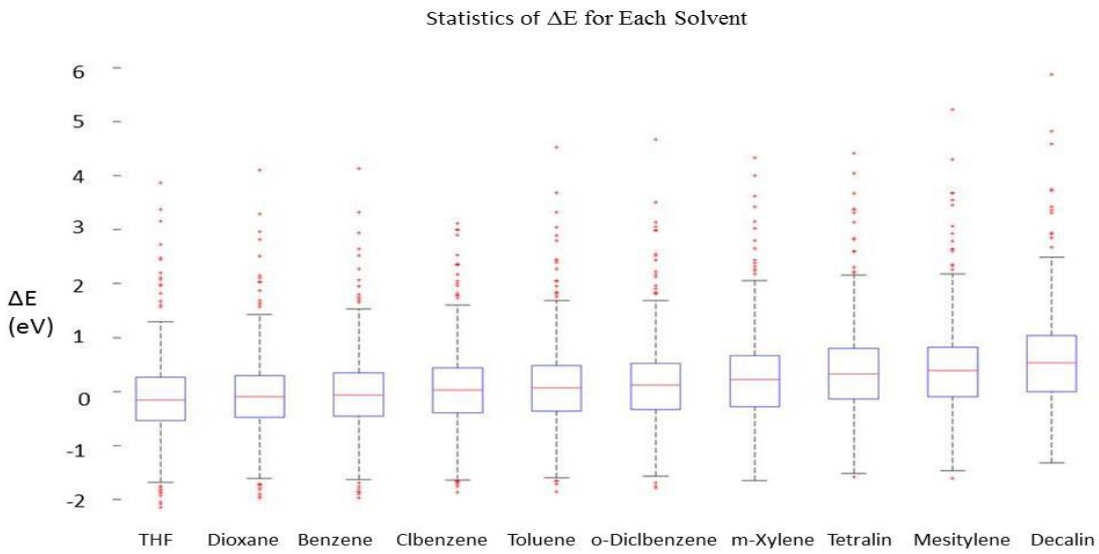

Figure 3.2b. Statistical data of ΔE for each solvent.

The effect of the presence of the single LJ atom on deviations in the acene backbone of the TIPS pentacene molecules nearby (defined in **Figure 3.3**) away from those for the equilibrium unit cell configuration (without solvent) was also studied. The mean and median (and the standard deviation) of all the acene angle and side group angle changes over the entire range of [a, b, γ] parameters that were studied were calculated for each of the solvents and plotted against the solvent radius (see **Figure 3.4**). From **Figure** 3.**4**, it can be seen that changes in the angle formed by C1-C2-C3 (side A), which are three carbon atoms on the acene backbone, as the inserted LJ atom increases in size are more significant than the corresponding angle on the other side of the backbone (side B), C3-C4-C5. Side A demonstrated an acene backbone bend of 1-3º, becoming increasingly bent as the size of the LJ solvent atom increases. In contrast, side B showed only about 1º of bend on average and this does not change as the size of the LJ atom is increased. Thus, the bending of the molecule is quite localized, and the acene bends and twists slightly (see **Figure 3.5**). The linearity of the changes in angle for the acene backbone angle with respect to the solvent radius indicate that the acene bending and twisting have an impact on the energy profile.

The linearity of the change in energy against the solvent radii can be seen when looking at all of the polymorphs for each of the solvents (see **Figures 3.6 – 3.10**). The five minima for 6,13-TIPS pentacene in each solvent were determined; the energy of the crystal using the parameters assigned by Giri *et al*. without solvent was used as the base line.

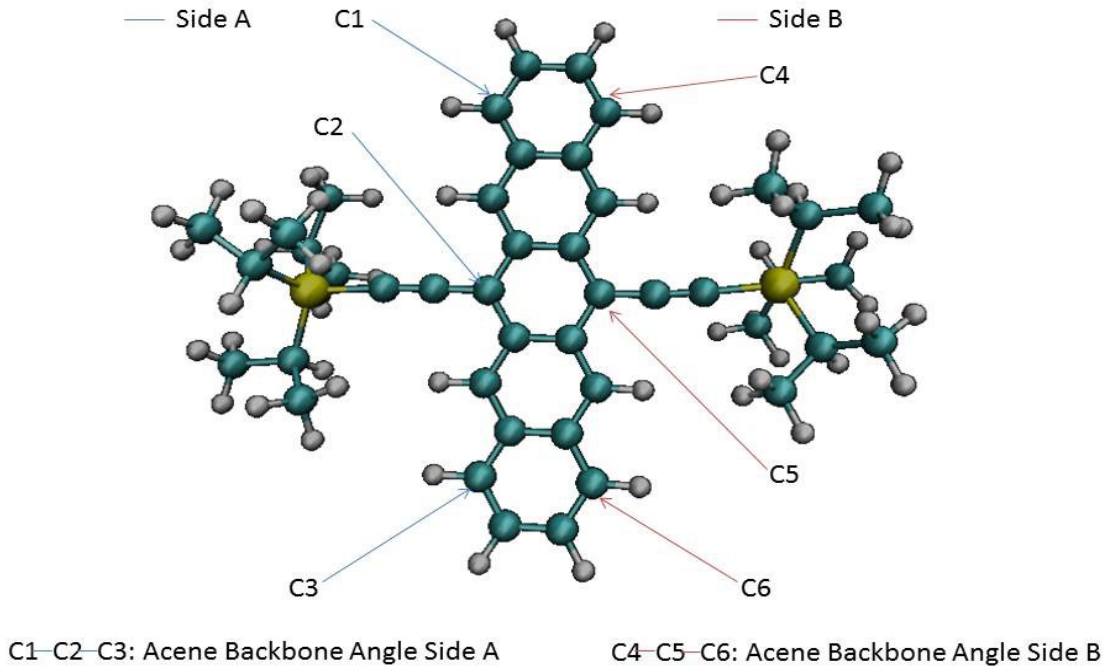

Figure 3.3. Schematic of the TIPS-Pn molecule identifying (a) the sides of the acene backbone angles as side A (blue lines point to the side implicated as "A") or side B (red lines). Lines connecting the atoms labeled as C1, C2, and C3 determine the angle calculated to determine the bend in the acene backbone on side A; atoms C4, C5, and C6 form the corresponding angle on side B.

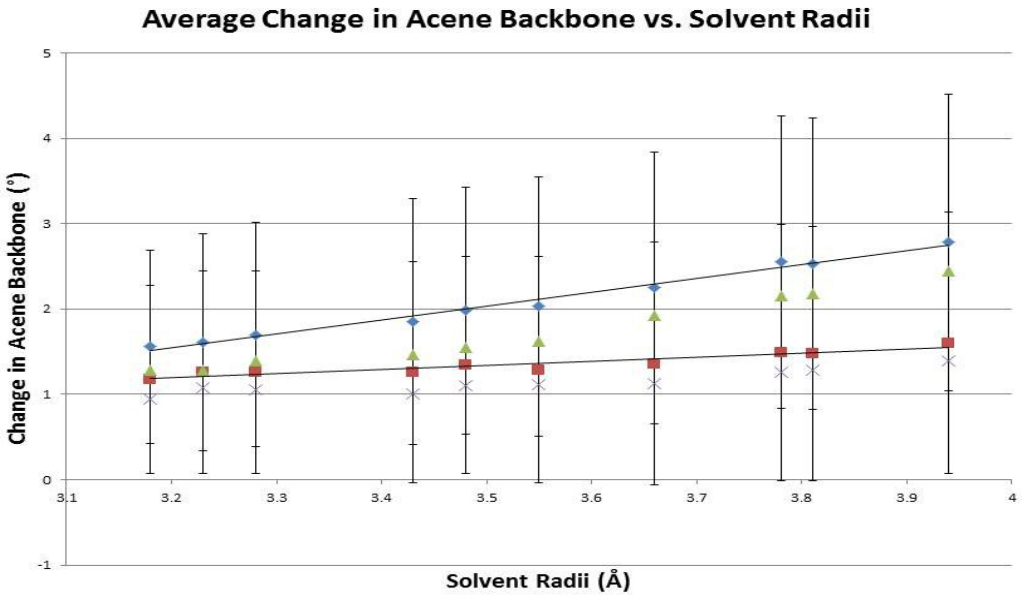

Figure 3.4. Change in acene backbone angle vs. solvent radii. The mean change in acene backbone angle for sides A and B are shown as blue and red symbols, respectively, connected by a linear trend line. The median changes are shown as green and purple symbols for sides A and B, respectively.

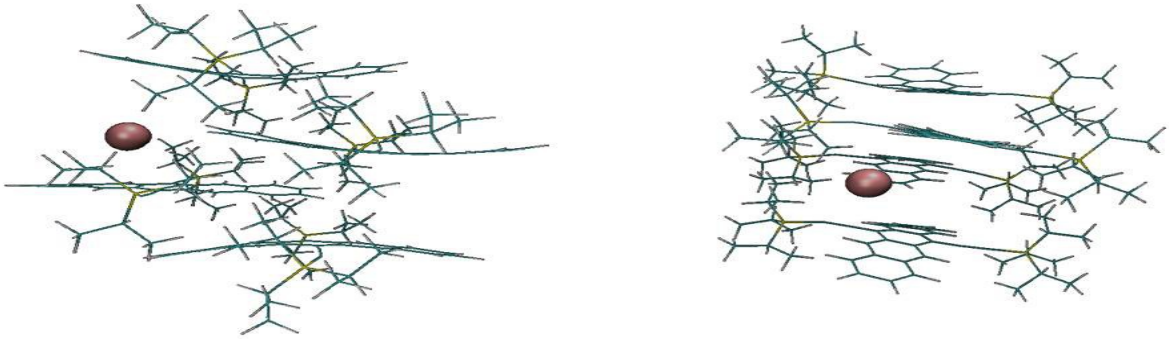

Figure 3.5. Two snapshots from the energy minimization of the TIPS-Pn unit cell in the presence of the LJ atom (brown sphere) showing the bending and twisting in the acene backbone that the atom induces by its presence.

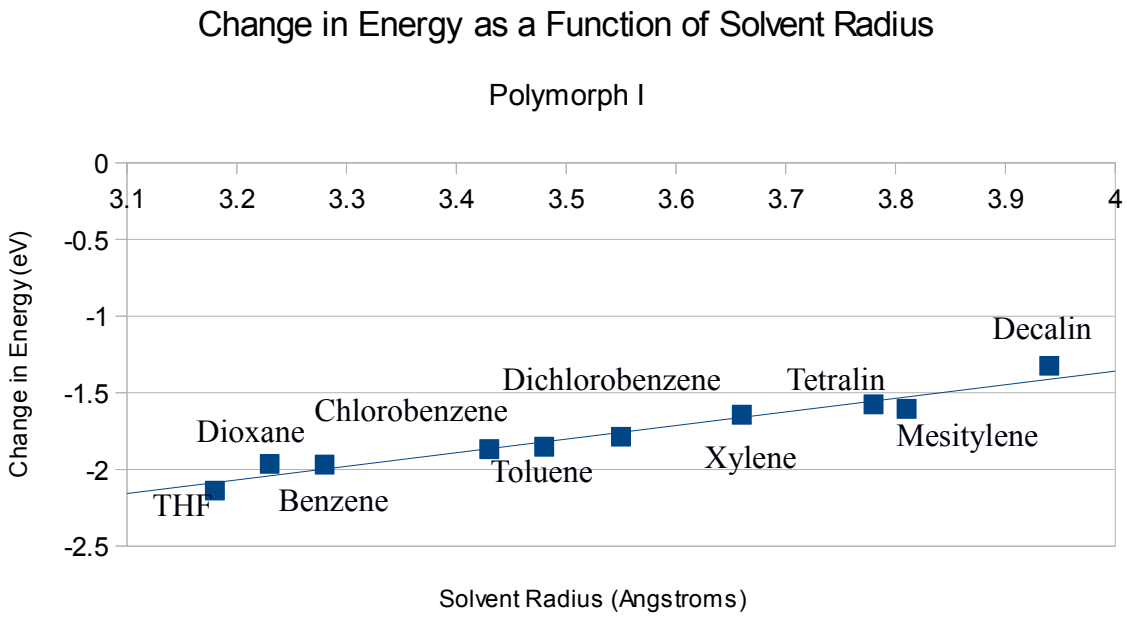

Figure 3.6. The energy minima for Polymorph I for each solvent.

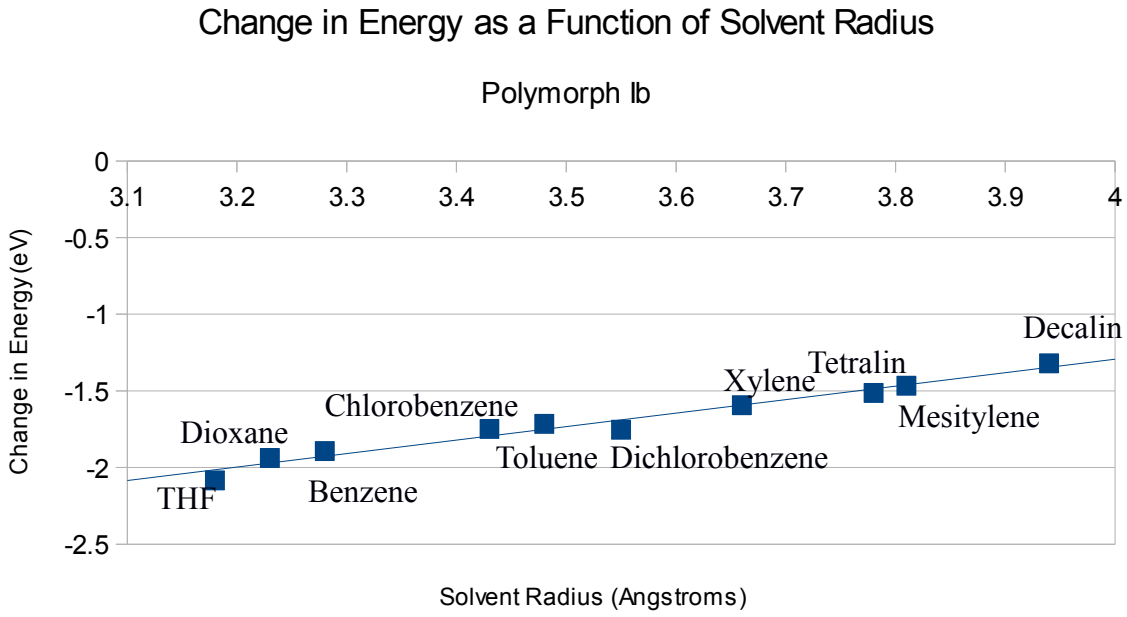

Figure 3.7. The energy minima for Polymorph Ib for each solvent.

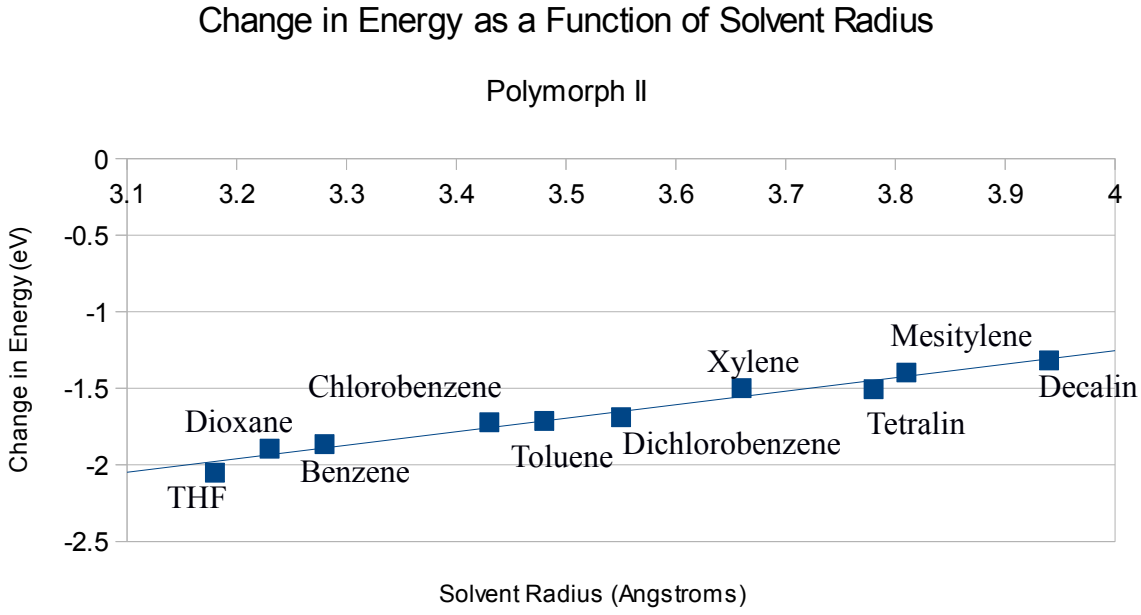

Figure 3.8. The energy minima for Polymorph II for each solvent.

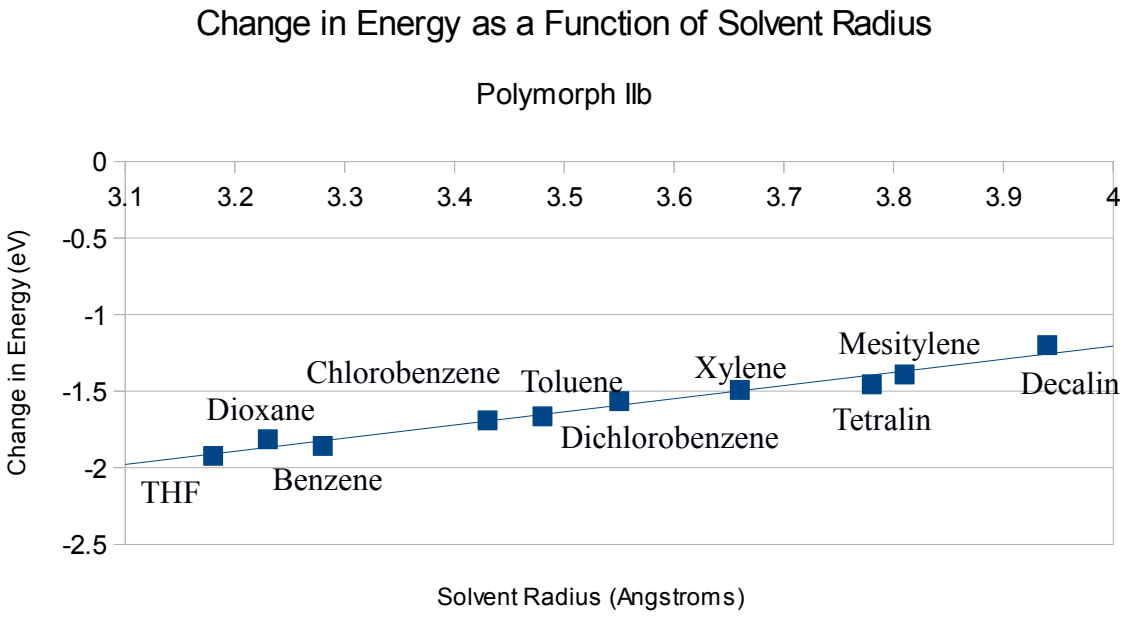

Figure 3.9. The energy minima for Polymorph IIb for each solvent.

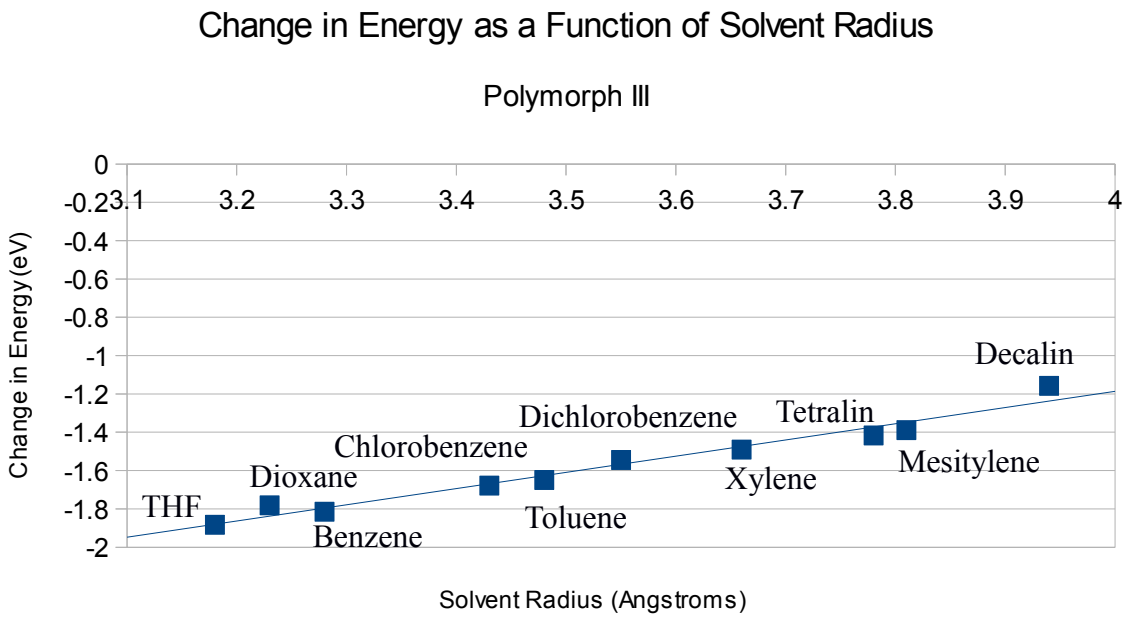

Figure 3.10. The energy minima for Polymorph III for each solvent.

REFERENCES

1. http://avogadro.openmolecules.net/wiki/Main_Page

2. http://gaussian.com/

3. http://dasher.wustl.edu/tinker/

4. Giri, G., E. Verploegen, S. C. B. Mannsfeld, S. Atahan-Evrenk, D. H. Kim, S. Y. Lee, H. A. Becerril, A. Aspuru-Guzik, M. F. Toney, Z. Bao. "Tuning charge transport in solution-sheared organic semiconductors using lattice strain." *Nature* 2011, **480**.

CHAPTER 4

CONCLUSION AND FUTURE WORK

Conclusions

The focus of this work is a computational determination of the energy profiles of the organic semiconductor molecule, 6,13-TIPS pentacene, and its changes with respect to variations in the [a,b,γ] unit cell parameters. Using MM3 models and energy minimization techniques of a search of the [a,b,γ] space, it was observed that it is possible to identify all five of the polymorphs (I, Ib, II, IIb, and III) observed experimentally as mapping to the five lowest energy structures that were found. This semi-empirical model had been parameterized against *ab initio* data that were generated for interactions within the molecule that were not available in the TINKER database. Given the conformational flexibility mentioned above, this is by no means a foregone conclusion. The quality of the reproduction of the polymorphs provided the confidence to investigate the molecular origin driving their formation.

It was also found that there was a correlation between minimizing the strain in the molecule and the location in [a,b,γ] space of the major polymorphs. As the [a,b,γ] parameters values were changed, it was observed that the acene backbone bends and twists, the methyl groups and the silyl-ethynyl angle in the TIPS functional group rotate. Determining which of these three structural changes (backbone distortion, methyl group rotation or TIPS group wagging) is primarily responsible is not completely clear. However, several observations helped to create a reasonable picture

of the sequence of events that lead to the energetic preference of a particular polymorph.

First, the largest strain is encountered when the TIPS group wags or rotates. Second, the degree of twisting observed here in the acene backbone was not observed in earlier computational studies of the parent pentacene molecules. This suggests that the acene backbone changes are an effect rather than a cause. Given the steric "bulk" of the TIPS group this conclusion seems intuitively reasonable. Piecing this information together, it is possible that this is a "domino effect:" the methyl groups that constitute the TIPS group rotate, but work against each other on opposite sides of the pentacene backbone. This causes the silyl-ethynyl groups to wag. As one side wags, the other side approaches the equilibrium angle. Eventually, they begin to work together, but they induce strain into the acene backbone causing it to bend and twist. This possibly affects the energy landscape. Evidence for this connection between minimizing strain in the TIPS-pentacene molecule and the energy landscape is provided when it is considered that the minima for the angular differences (*i.e.,* a minimization of the strain) align closely with the minima of the energy profiles.

The effects of solvent size on the energy profile is also important to this study. A Lennard-Jones atom was placed within each of the configurations mentioned above and its size varied so that it represented solvents from tetrahydrofuran to decalin. The dependence of the average change in energy on the size of the solvent produced a linearly increasing trend. As the solvent size increases, the more unstable the equilibrium crystal structure becomes. This instability may be caused by the localized

strain that the Lennard-Jones atom places on the acene backbone. As the solvent size increases, the bending and twisting of the acene angle on one side of the TIPS-pentacene molecule increases linearly; therefore, the strain on the molecules follows the same trend as the change in energy in relation to the solvent size.

Future Work

This project could progress by observing, via molecular dynamics, how the molecular orientation evolves as the system is sheared at a constant velocity. Giri *et al*. reported using shearing velocities between 0.4 and 8 mm/s [1]. Accessible length and time scales in MD are angstroms and tens of nanoseconds, respectively, which "translates" to velocities on the order of $1e^{-2}$ Å in a 10-ns simulation.

Chynoweth *et al*. developed an MD algorithm suitable for studying organic materials (specifically, lubricants) under shear. One of the issues with shearing a structure using MD is how to account for periodic boundary conditions [2]. For cubic structures, a Ewald sum is usually employed; however, Lees-Edwards boundary conditions can be applied to a system under shear, taking into account the changing boundary [3]. Another issue regarding shear in MD simulations is that a temperature gradient can be induced at large shear rates, which is problematic when running simulations employing a thermostat. To circumvent this issue, the SLLOD equations of motion can be used, which are a set of perturbed equations of motion that allow the system to remain at a constant temperature and can be applied to spatially homogeneous systems [4].

To properly study the shearing effects on 6,13-TIPS pentacene, the bottom two

molecules could be fixed with a constant shear rate applied in the direction of the b-axis to the top two molecules; the Large-scale Atomic/Molecular Massively Parallel Simulator (LAMMPS) simulation engine will need to be used, which, unlike TINKER, can handle the SLLOD equations of motion and can utilize a similar approach to the Lees-Edwards boundary conditions.

The analysis of these structures will involve observing how the energy is affected by the changing unit cell angle and comparing the energy for one angle at one applied shear rate against all other rates. Also, determining the relationship between the energy and the changing the a- and b-axes will be undertaken.

From Vacuum Conditions to a Solvated Structure

The original experimental observation by the Bao group of the equilibrated and metastable structures of 6,13-TIPS pentacene involved the introduction and evaporation of toluene solvent. Hence, another step in this project will involve studying the behavior of 6,13-TIPS pentacene undergoing shear in a toluene solvent.

Chen *et al*. performed an experimental study that tested the solubility of 6,13-TIPS pentacene in a series of organic solvents, which revealed that it is most soluble in toluene. Also, because of toluene's high boiling point, its evaporation could be controlled to form larger crystals and hence was the obvious choice for the Bao group's study [5]. Park *et al*. studied different solution deposition methods using different solvents and how each one affects the field-effect mobility for the organic

thin film transistor using 6,13-TIPS pentacene. They determined that, of the methods and solvents tested, drop casting using a toluene solvent yielded the highest field-effect mobility (1.2 cm2/Vs) [6].

The next task will be to model a vapor-liquid interface between the unit cell of 6,13-TIPS pentacene and toluene vapor. The simulations would allow us to be able to visualize and comprehend how the interactions of toluene with 6,13-TIPS pentacene can stabilize the unit cell at an equilibrium configuration and how its absence significantly reduces the system's stability.

In order to study the effects of toluene on the dynamics behind the transition from a metastable to an equilibrated state, the energy-minimized unit cell and sufficient toluene molecules to cover the top of the two molecules to which the velocity would be applied would be isolated. The toluene layer will be large enough so that (if shear were being applied) the top two molecules would remain covered for the longest values of the a- and b-axes and the largest value for γ.

After each configuration has been energy-minimized, they will also be equilibrated but separately at first; this is to allow each structure to be able to come to a "steady" configuration at the required temperature without interfering with each other. The toluene will be equilibrated as a vapor, and 6,13-TIPS pentacene will be equilibrated as a liquid. Once they have both equilibrated, the two "layers" will be combined and form a vapor-liquid interface, NPT (constant pressure and temperature) simulations will be performed, and the energy with respect to simulation time step will be observed. In addition, determining how the unit-cell angle and the lengths of the a-

and b-axes change will be investigated.

This is an initial investigation working under the assumption that since the bottom two TIPS molecules remain fixed during the shearing process, surrounding them with toluene vapor may not be necessary. However, toluene is the solvent in the solution being sheared; the reorganization observed by the Bao group could be due to toluene providing some sort of stability to all of the atoms in the system.

To observe the solvated 6,13-TIPS pentacene system under shear, the previous two calculations will be combined by first minimizing and equilibrating liquid 6,13-TIPS pentacene and toluene vapor and then combining them. Once the two are brought together (whether as two separate "layers" or as a fully-solvated system, depending on what will be determined from the previous calculation), they will be equilibrated and a constant shearing velocity in the direction of the b-axis will be applied to the top two molecules. The relationship between the change in unit-cell conformation and the energy will be determined and compared against what was found for the system *in vacuo*.

Parameterization

In order to study this in LAMMPS, the system will need to be re-parameterized as MM3 is not supported in LAMMPS. Instead, OPLS could be used to model the bond lengths, angles, and dihedrals. The same steps for parameterizing 6,13-TIPS pentacene in MM3 will need to be used in OPLS. Whatever bond lengths and angles are unknown, a Gaussian09 optimization calculation will need to be run to obtain the equilibrium parameters. Then, the bond lengths will need to be stretched

and contracted and the bond angles will need to be bent; each configuration will be submitted to a single-point energy calculation in Gaussian09 and the data fitted against the bond stretching and angle bending equations for OPLS.

REFERENCES

1. Giri, G., E. Verploegen, S. C. B. Mannsfeld, S. Atahan-Evrenk, D. H. Kim, S. Y. Lee, H. A. Becerril, A. Aspuru-Guzik, M. F. Toney, Z. Bao. "Tuning charge transport in solution-sheared organic semiconductors using lattice strain." *Nature* 2011, **480**: 504 – 508.

2. Hanson, A. J. *Visualizing Quaternions*. Amsterdam: Elsevier, 2006.

3. Chynoweth, S., U. C. Klomp, L. E. Scales. "Simulation of organic liquids using pseudo-pairwise interatomic forces on a toroidal transputer array." *Computer Physics Communications* 1991, **62**: 297 – 306.

4. Wheeler, D. R., N. G. Fuller, R. L. Rowley. "Non-equilibrium molecular dynamics simulation of the shear viscosity of liquid methanol: adaptation of the Ewald sum to Lees-Edwards boundary conditions." *Molecular Physics* 1997, **92**: 55 – 62.

5. Chen, J., D. C. Martin, J. E. Anthony. "Morphology and molecular orientation of thin-film bis(triisopropylsilylethynyl) pentacene." *Materials Research Society* 2007, **22**: 1701 – 1709.

6. Park, S. K., T. N. Jackson, J. E. Anthony, D. A. Mourey. "High Mobility Solution Processed 6,13-Bis(triisopropylsilylethynyl) Pentacene Organic Thin Film Transistors." *Applied Physics Letters*, 2007, **91**: 063514-1 - 063514-3.